Journal for
ImmunoTherapy of Cancer

IgA antibody immunotherapy targeting GD2 is effective in preclinical neuroblastoma models

Marjolein C Stip [1], Mitchell Evers,[1] Maaike Nederend,[1] Chilam Chan,[1] Karli R Reiding,[2,3] Mirjam J Damen,[2] Albert J R Heck,[2,3] Sofia Koustoulidou,[4] Ruud Ramakers,[4] Gerard C Krijger,[5] Remmert de Roos,[5] Edouard Souteyrand,[1] Annelisa M Cornel [1,6] Miranda P Dierselhuis,[6] Marco Jansen,[1] Mark de Boer,[7] Thomas Valerius [8] Geert van Tetering,[1] Jeanette H W Leusen [1] Friederike Meyer-Wentrup[6]

For numbered affiliations see end of article.

Correspondence to
Dr Jeanette H W Leusen;
j.h.w.leusen@umcutrecht.nl

ABSTRACT

Background Immunotherapy targeting GD2 is very effective against high-risk neuroblastoma, though administration of anti-GD2 antibodies induces severe and dose-limiting neuropathic pain by binding GD2-expressing sensory neurons. Previously, the IgG1 ch14.18 (dinutuximab) antibody was reformatted into the IgA1 isotype, which abolishes neuropathic pain and induces efficient neutrophil-mediated antibody-dependent cellular cytotoxicity (ADCC) via activation of the Fc alpha receptor (FcαRI/CD89).

Methods To generate an antibody suitable for clinical application, we engineered an IgA molecule (named IgA3.0 ch14.18) with increased stability, mutated glycosylation sites and substituted free (reactive) cysteines. The following mutations were introduced: N45.2G and P124R (CH1 domain), C92S, N120T, I121L and T122S (CH2 domain) and a deletion of the tail piece P131-Y148 (CH3 domain). IgA3.0 ch14.18 was evaluated in binding assays and in ADCC and antibody-dependent cellular phagocytosis (ADCP) assays with human, neuroblastoma patient and non-human primate effector cells. We performed mass spectrometry analysis of *N*-glycans and evaluated the impact of altered glycosylation in IgA3.0 ch14.18 on antibody half-life by performing pharmacokinetic (PK) studies in mice injected intravenously with 5 mg/kg antibody solution. A dose escalation study was performed to determine in vivo efficacy of IgA3.0 ch14.18 in an intraperitoneal mouse model using 9464D-GD2 neuroblastoma cells as well as in a subcutaneous human xenograft model using IMR32 neuroblastoma cells. Binding assays and PK studies were compared with one-way analysis of variance (ANOVA), ADCC and ADCP assays and in vivo tumor outgrowth with two-way ANOVA followed by Tukey's post-hoc test.

Results ADCC and ADCP assays showed that particularly neutrophils and macrophages from healthy donors, non-human primates and patients with neuroblastoma are able to kill neuroblastoma tumor cells efficiently with IgA3.0 ch14.18. IgA3.0 ch14.18 contains a more favorable glycosylation pattern, corresponding to an increased antibody half-life in mice compared with IgA1 and IgA2. Furthermore, IgA3.0 ch14.18 penetrates neuroblastoma

WHAT IS ALREADY KNOWN ON THIS TOPIC

⇒ Previously, the IgG1 ch14.18 (dinutuximab) antibody was reformatted into the IgA1 isotype, which abolishes neuropathic pain and induces efficient neutrophil-mediated tumor killing. However, this IgA1 format was not ready for clinical application yet, since (1) the *O*-glycosylation in IgA1 antibodies is associated with the development of Berger's disease, (2) IgA1 has a short half-life and (3) IgA1 is not stable, which complicates production and purification of a clinical batch.

WHAT THIS STUDY ADDS

⇒ In this study we developed a novel format of IgA anti-GD2 immunotherapy (IgA3.0 ch14.18), which is suitable for clinical application since it lacks *O*-glycosylation, has an increased half-life and enhanced stability.

HOW THIS STUDY MIGHT AFFECT RESEARCH, PRACTICE OR POLICY

⇒ IgA3.0 ch14.18 could replace the current immunotherapy for neuroblastoma (IgG1 ch14.18, dinutuximab), since IgA3.0 ch14.18 is at least as efficacious and does not induce severe neuropathic pain.

tumors in vivo and halts tumor outgrowth in both 9464D-GD2 and IMR32 long-term tumor models.

Conclusions IgA3.0 ch14.18 is a promising new therapy for neuroblastoma, showing (1) increased half-life compared to natural IgA antibodies, (2) increased protein stability enabling effortless production and purification, (3) potent CD89-mediated tumor killing in vitro by healthy subjects and patients with neuroblastoma and (4) antitumor efficacy in long-term mouse neuroblastoma models.

BACKGROUND

Neuroblastoma is a pediatric tumor originating from dysregulation of the development of neural crest cells from the

sympathoadrenal lineage.[1] A distinctive characteristic of neuroblastoma is the high heterogeneity in disease severity. Whereas the 5-year survival rate of low-risk and intermediate-risk neuroblastoma can be up to 95%, only 45% of patients with high-risk neuroblastoma live longer than 5 years. Currently, after an extensive treatment regimen containing chemotherapy, surgery, radiation therapy and hematopoietic stem cell transplantation,[2 3] high-risk patients can receive immunotherapy. This immunotherapy encompasses anti-GD2 IgG antibodies, of which dinutuximab (IgG1 ch14.18), a chimeric antibody directed against the ganglioside GD2, was the first clinically approved antibody. Anti-GD2 immunotherapy is currently combined with granulocyte-macrophage colony-stimulating factor (GM-CSF, when available) and 13-cis retinoic acid.[4] The addition of immunotherapy to the treatment regimen improved event-free survival by 20%, but unfortunately induces severe neuropathic pain, probably evoked through complement activation on GD2-expressing sensory neurons.[4] Though long-term infusion strategies were introduced to reduce pain, still 37.7% of the patients experiences grade $\geq$3 neuropathic pain.[5] Anti-GD2 antibodies inhibit tumor growth mainly by inducing antibody-dependent cell-mediated cytotoxicity (ADCC). Natural killer (NK) cells are often considered to be the most important effector cells performing ADCC, but in neuroblastoma immunotherapy neutrophil-mediated ADCC plays a major role as well.[6–10] Additionally, anti-GD2 antibodies activate the complement system on GD2-expressing tumor cells via its C1q binding domain. This effector mechanism appears less important than ADCC though, since an Fc point mutation in the C1q domain (K322A) abolishing complement-dependant cytotoxicity does not reduce therapeutic efficacy in patients.[11 12]

Previously, IgG1 ch14.18 (dinutuximab) was reformatted to the IgA1 isotype and it was observed that this abolishes neuropathic pain in a mouse model and induces efficient neutrophil-mediated ADCC through activation of the Fc alpha receptor (FcαRI, CD89).[13] Human IgA antibodies are naturally occurring in two isotypes—IgA1 and IgA2—with three possible allotypes for IgA2 (IgA2m(1), IgA2m(2), and IgA2n).[14 15] IgA1 and IgA2 molecules contain 2 and 4–5 N-glycosylation sites respectively, whereas IgG1 only has one.[16] This extensive glycosylation contributes to the short half-life of endogenous IgA (4–7 days)[17 18] compared with endogenous IgG (ranging from 11 to 30 days)[19] and monoclonal IgG1 antibodies (21 days).[20 21] In mice, IgA half-life is even shorter (15 hours).[22] First, this short half-life is caused by fast clearance of IgA in the distribution phase by the asialoglycoprotein receptor (ASGPR),[22–24] recognizing asialylated galactoses on proteins. Second, clearance can occur via the mannose receptor (CD206), which binds terminal mannose glycan structures.[25 26] Third, IgA antibodies lack a binding site for the neonatal Fc receptor (FcRn) and are thereby not recycled by FcRn, while IgG antibodies are.[27–29]

To bring IgA ch14.18 to the clinic, we have taken several steps in this study to improve the format, which we named IgA3.0 (figure 1A). The IgA3.0 format is a next generation engineered IgA molecule based on the IgA2.0 molecule as described and studied previously by Lohse and colleagues.[30–32] First of all, the IgA3.0 antibody is a derivative of the IgA2 isotype, since IgA1 antibodies can be critically involved in the development of IgA nephropathy (Berger's disease) mediated by aberrant O-glycosylation sites in the hinge region.[33] Second, we aimed to reduce antibody clearance by the ASGPR and mannose receptor, by reducing the absolute amount of glycosylation. To achieve this, N45.2G (CH1) and N120T (CH2) mutations were introduced at these N-glycosylation sites.[32] The penultimate glycosylation site (N135) was removed by a complete deletion of the tail piece, leaving only the glycosylation site at N20 in the CH2 domain. Since the tail piece is critically involved in dimerization of IgA,[34] it was deleted to prevent aggregation. Third, the P124R mutation in the CH1 domain was introduced to stabilize the pairing of heavy chain (HC) and kappa light chain (κLC)[30] and free cysteines were substituted or removed by tail piece deletion. In this study, we first characterized the novel IgA3.0 ch14.18 antibody and compared it to the original IgG1 and unmodified IgA1 and IgA2 formats. We performed functional assays (ADCC and antibody-dependent cell-mediated phagocytosis (ADCP)) with effector cells from healthy donors, non-human primates and patients with neuroblastoma and compared the formats in pharmacokinetic (PK) studies, mass spectrometry and thermal stability tests. Next, we evaluated the efficacy of IgA3.0 ch14.18 in long-term preclinical neuroblastoma mouse models.

METHODS

Antibody design and production

Variable sequences of the ch14.18 HC and κLC were derived from Biologic License Application 125516 and cloned into expression vectors (pEE14.4) containing the κLC or HC of IgA1, IgA2m(1), IgA3.0 or IgG1. The IgA3.0 amino acid sequence is based on the IgA2m(1) sequence and contains the following mutations (according to ImMunoGeneTics (IMGT) unique numbering for C domain): in the CH1 domain N45.2G and P124R, in the CH2 domain C92S, N120T, I121L and T122S and in the CH3 domain a deletion of the tail piece P131-Y148. Subsequently, all antibody variants were produced by transient transfection of HEK293 Freestyle (HEK293F) cells with HC, κLC and pAdvantage (U47294; Promega) encoding vectors using 293fectin (Thermo Fisher). Additionally, IgG1 and IgA3.0 antibodies were produced in Expi-CHO-S (Chinese Hamster Ovarian) cells (using the Expi-CHO-S transfection kit) and in CHO-K1 cells (produced and purified by WuXi Biologics). In-house produced antibodies were isolated from filtered culture supernatants and purified by affinity and size-exclusion chromatography as described before.[13]
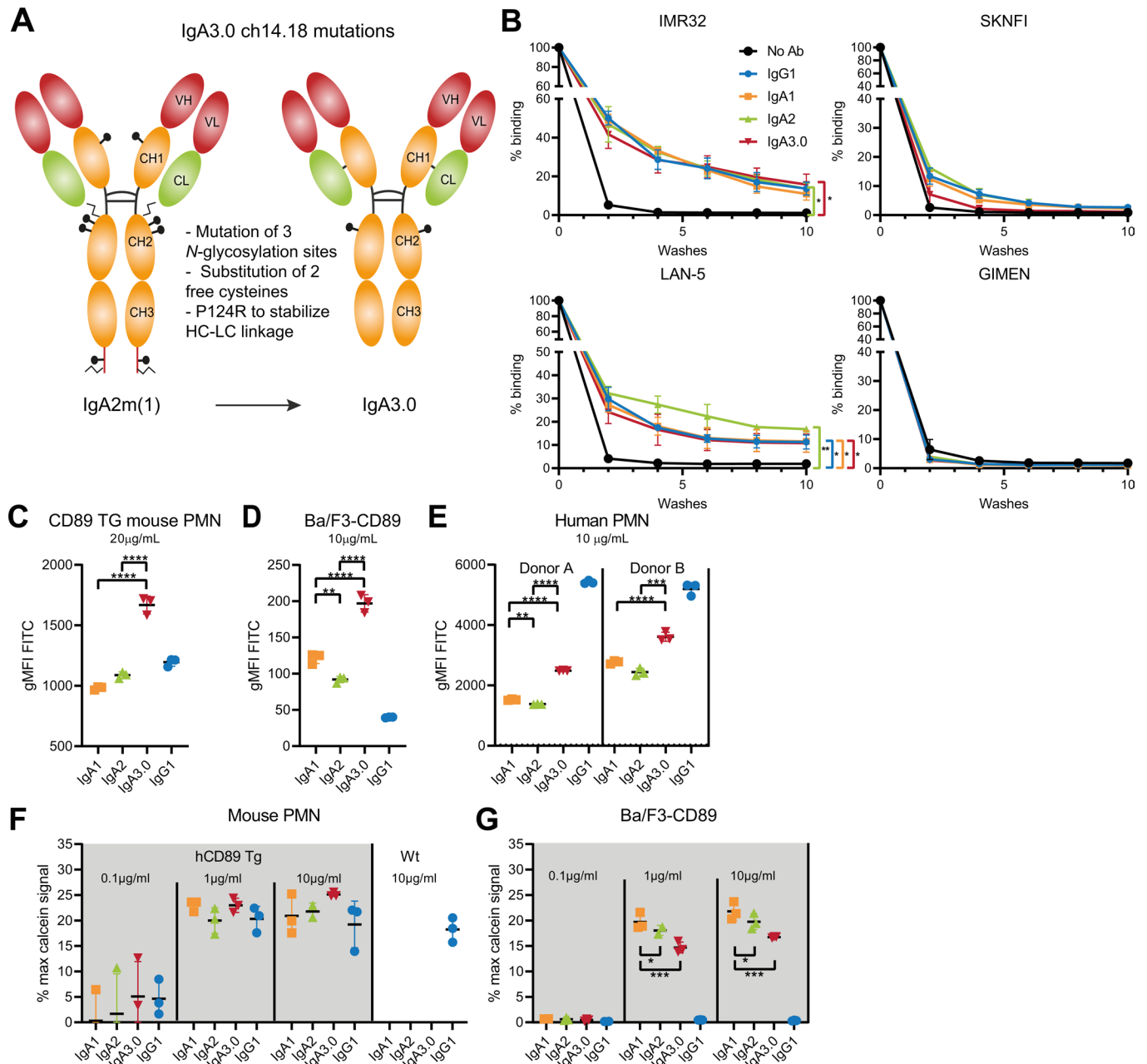
Figure 1 Characterization of IgA3.0 ch14.18 target (Fab) and Fc binding. (A) Description of mutations in the IgA3.0 molecule compared to the original IgA2m(1) antibody.[32] (B) Target-specific binding was measured by incubating calcein-labeled neuroblastoma cells on antibody-coated plates and measuring residual fluorescence after several washes. Binding was compared using a Repeated Measurements one-way ANOVA. Monomeric Fc-binding to CD89 was assessed by incubating ch14.18 antibodies with (C) CD89 transgenic mouse neutrophils, (D) Ba/F3-CD89 cells or (E) human PMN followed by detection with FITC anti-human kappa antibody. Binding of complexed IgA to CD89 was assessed by incubating calcein-labeled (F) CD89 transgenic mouse neutrophils or (G) Ba/F3-CD89 cells on antibody-coated plates and measuring remaining fluorescence after 10 washes. Monomeric binding was compared using a one-way and complexed binding using a two-way ANOVA. Data as shown are mean±SD, n=3 for all experiments. GD2 binding experiments were repeated five times, CD89 binding experiments were repeated twice. *p<0.05, **p<0.01, ***p<0.001 and ****p<0.0001. ANOVA, analysis of variance; FITC, fluorescein isothiocyanate; hCD89 Tg, human CD89 transgenic mice; PMN, polymorphonuclear leukocytes; Wt, wildtype mice.

Generation of fluorescently labeled antibodies

Antibodies were labeled with *N*-hydroxy-succimidyl-fluorescein isothiocyanate (NHS-FITC, Thermo Fisher) at room temperature (RT) for 2 hours while stirring. Unbound NHS-FITC and unlabeled antibody was removed by size-exclusion using Sephadex columns (NAP-5, GE Healthcare). AF594-labeled antibodies were generated using the Alexa Fluor 594 protein labeling kit (Thermo Fisher).

Cell culture

Human neuroblastoma cell lines were acquired from the American Type Culture Collection (ATCC) and cultured in Dulbecco's modified eagle medium (DMEM). Mouse 9464D neuroblastoma cells (derived from the National Institutes of Health) were a kind gift from Dr. Juliet Gray (University of Southampton) and were cultured in Roswell Park Memorial Institute (RPMI) medium. All neuroblastoma culture media were supplemented with HEPES, Glutamax, 10% heat-inactivated fetal calf serum (FCS, Bodinco), 100 U/mL penicillin-streptomycin (p/s, Gibco) and 2% non-essential amino acids (Thermo Fisher). Ba/F3 and HEK293T cells were cultured in RPMI supplemented with 10% FCS and 1% p/s. Additionally, 0.1 ng/mL murine interleukin (IL)-3 (Immunotools) was added to Ba/F3 cultures. All cells were cultured at 37°C in a humidified incubator containing 5% CO_2. HEK293F and Expi-CHO-S cells were cultured in respectively Free-Style-293 and ExpiCHO expression medium (Gibco) at 37°C in a humidified incubator with orbital shaker platform containing 8% CO_2. Cells were not cultured past 20 passages and they were tested every 6 weeks using a Mycoalert mycoplasma detection kit (Lonza). Authenticity of 9464D cells was confirmed by STR (short-tandem repeat) profiling.

Virus production and transductions

A bacterial stab containing the MP9956:SFG.GD3synthase-2A-GD2synthase (Addgene Plasmid #75013) DNA construct was expanded at 37°C in LB medium (MP Biomedicals) and DNA was purified using the NucleoBond Xtra Maxi kit (Macherey-Nagel). Next, 0.9 µg MP9956:SFG.GD3synthase-2A-GD2synthase construct, 0.1 µg of pCL-Ampho Retrovirus Packaging construct and 2.5 µL Fugene was added to 100 µL RPMI medium and complexed for 30 min at RT. For Luc2 transductions, 3 µg DNA constructs (pS-Luc2-T2A-GFP-P2A-BSD (transfer vector), pMDIg/p-pRRE, pRSV-REV pMD2-VSVg) and 1 mg/mL PEI (in 25 mM Hepes, pH 7.5, 150 mM NaCL) were added to 100 µL OptiMEM and complexed for 30 min at RT. For virus production, 3×10^5 adherent HEK293T cells in a 6-well plate were transfected with one of the DNA mixes. Virus supernatant was harvested after 48 hours and 72 hours.

Forty per cent confluent 9464D or GIMEN cells were transduced with 3 mL virus supernatant containing 6 µg/mL polybrene (Sigma) and centrifuged for 2 hours at 1000× g at 33°C. GD2-expressing clones were selected after limiting dilutions by staining with AF594-labeled ch14.18 and subsequent flow cytometric analysis. Luc2-positive cells were positively selected by culturing in 10 µg/mL blasticidin (InvivoGen).

Target and CD89 binding assays

For assessment of target-specific binding, ch14.18 antibodies were coated overnight in carbonate-bicarbonate buffer (Sigma) at 4°C on NUNC MaxiSorp 96-well plates (Thermo Fisher). After blocking with 1% bovine serum albumin (BSA, Roche) in phosphate-buffered saline (PBS), 1.5×10^5 cells/100 µL/well calcein-labeled neuroblastoma cells were added, centrifuged for 5 min at 300 rpm and incubated for 30–45 min at 37°C and 5% CO2. Thereafter, cells were washed 10 times and after every two washes fluorescence was measured on a Spectramax (excitation: 485 nm, emission: 527 nm).

For assessment of monomeric Fc binding, 1×10^5 Ba/F3-CD89 cells, murine bone marrow-derived neutrophils (C57BL/6, transgenic for human CD89) or human polymorphonuclear leukocytes (PMN) were incubated with a range of concentrations of ch14.18 variants for 45–60 min at 4°C. After washing, samples were incubated with anti-human kappa FITC antibody for 30–45 min at RT, washed and analyzed using a FACSCanto II. For assessment of complexed Fc binding, the target binding assay as described above was performed, but now Ba/F3-CD89 cells and murine neutrophils were used instead of neuroblastoma cells.

ADCC assays

^{51}Cr-release assays were performed as described previously.[35] In short, target cells were labeled with radioactive chromium-51 ($Na_2^{51}CrO_4$, PerkinElmer) and washed three times. Whole blood leukocytes (WBL) were isolated by incubating blood samples in water for 30 s to lyse erythrocytes, after which 10× PBS was added. PMN and peripheral blood mononuclear cells (PBMC) were isolated using Ficoll (GE Healthcare)/Histopaque 1119 (Sigma) density gradient centrifugation and subsequent erythrocyte lysis using red blood cell (RBC) Lysis Buffer (BioLegend). PMN and PBMC composition was determined using the antibody panel in online supplemental table 1 and 2 followed by analysis on the LSRFortessa (BD). Cynomolgus PMN were isolated similarly from cynomolgus blood samples collected at Covance, Germany. Mouse neutrophils were isolated from blood collected 4 days after subcutaneous (s.c.) injection of PEGylated granulocyte colony-stimulating factor (G-CSF, 20 µg/mouse). Murine neutrophils were isolated by performing erythrocyte lysis (BioLegend), followed by magnetic separation using anti-Ly-6G Microbeads (Miltenyi) according to manufacturer's instructions.

PBMC were added in a 100:1 effector-target (E:T) ratio and PMN or mouse neutrophils in a 40:1 ratio (ratios determined in previous studies[35]). Antibodies were added in concentrations as indicated per experiment. Assays were incubated for 4 hours at 37°C in a humidified incubator containing 5% CO_2. Plates were centrifuged and supernatant was transferred to lumaplates (PerkinElmer) to assess radioactivity induced scintillation (in cpm) on a beta-gamma counter (PerkinElmer). Specific lysis was calculated using the formula: ((experimental cpm – basal cpm)/(maximal cpm – basal cpm))×100, with maximal lysis determined by incubating target cells with 1.25% triton and minimal lysis determined by chromium release of target cells in the absence of antibodies and effector cells.

Phagocytosis assays and confocal imaging

Human monocytes were isolated from PBMC using CD14 microbeads (Miltenyi) and cultured for 7–14 days in the presence of 20 ng/mL rhM-CSF (Gibco) or rhGM-CSF (Miltenyi). When indicated, macrophages were further polarized for 24 hours with 20 ng/mL IL-4 (Immunotools), 50 ng/mL interferon (IFN)-γ (Thermo Fisher) or 5 µM NECA (Santa Cruz). Target cells were labeled with pHrodo-AM (Thermo Fisher) and macrophages with CellTrace Violet (CTV, Thermo Fisher), both according to manufacturer's instructions. Macrophages were added in a 1:2 E:T ratio and antibodies were added in indicated concentrations. After 3 hours, cells were detached using accutase (Sigma) and analyzed by flow cytometry (LSRFortessa).

Target cells (IMR32) were labeled with pHrodo-AM and seeded in an 8 well µ-slide (Ibidi) 4 days prior to cell imaging. Subsequently, 10 µg/mL FITC-labeled anti-GD2 antibodies and macrophage colony-stimulating factor (M-SCF) differentiated, CTV-labeled macrophages were added in a 1:2 E:T ratio. Images were taken using a Stellaris 5 confocal microscope (Leica), housed in a conditioned, temperature-controlled (37°C), humidified chamber containing 5% CO_2. Images were recorded using an HC PL APO 63x/1.40 OIL C immersion objective and analyzed using LAS X software (Leica).

Thermal shift assays

Volumes of 5 µL of 2.5 mg/mL antibody, 12.5 µL PBS and 7.5 µL 300× SYPRO orange (Invitrogen) were added in a 96-well PCR plate (BIOplastics). PCR plates were sealed with MicroAmp optical adhesive film (Thermo Fisher) and centrifuged to remove air. Plates were measured on a viiA7 Real-Time PCR system (Thermo Fisher) from 37°C up to 99°C with a ramp rate of 1°C/min. Samples were excited at 490 nm and fluorescence was measured at 575 nm. Melting temperatures (Tm values) are calculated by transforming temperature values to log(10) followed by non-linear regression (agonist vs response – find EC50) on the transformed data.

Glycoprofiling by mass spectrometry

N-Glycosylation profiles on ch14.18 antibody variants were analyzed using mass spectrometry as specified in detail in the online supplemental file 1.

Animal experiments

Mice were housed and bred at Janvier Labs (France) and transported to the animal facility of the Utrecht University (GDL) at least 1 week prior to the experiment. Food and water were provided ad libitum and mice were housed in groups under a 12:12 light–dark cycle. Mice were sacrificed by cervical dislocation. Both male and female mice from C57BL/6JRj, BALB/cByJ (both Janvier) and NXG (NOD.Cg-Prkdc^scid Il2rg^tm1Wjl/SzJ, Charles River) strains were used with age ranging from 8 to 30 weeks. Human CD89 transgenic mice were generated as described before,[36] subsequently backcrossed (15–40 generations)

into C57BL/6JRj, BALB/cByJ and NXG strains and maintained hemizygously. Mice in experimental groups were randomized based on weight, age and cage, researchers were single-blinded and group size was calculated a priori with a power of 0.8.

PK studies and antibody concentration measurement in mouse serum by ELISA

Female Balb/c and male NSG mice were injected intravenously (i.v.) with 5 mg/kg antibody solution in PBS and blood was sampled from the submandibular vein at indicated time points. Samples were left to coagulate overnight in Eppendorf tubes at 4°C. After centrifuging twice at 3000× g, serum was collected and stored at −20°C. MaxiSorp 96-well plates were coated with 0.5 µg/mL polyclonal goat-IgG anti-human kappa (1:2000, SouthernBiotech) in PBS overnight at 4°C. Next, plates were washed thrice with wash buffer (0.05% Tween20 in PBS) and blocked for 1 hour with 1% BSA in wash buffer. Serum samples and standards were diluted in PBS and incubated for 1.5 hours at RT. After washing thrice, polyclonal goat anti-human IgA/IgG-HRP (1:2000, SouthernBiotech) was added for 1 hour. After washing thrice again, plates were developed for 10 min with ABTS (Roche) and measured on a spectrophotometer (Bio-Rad) at 415 nm.

Mouse neuroblastoma models

IMR32 cells were diluted in a 1:1 mix of PBS and high concentration matrigel (Corning). CD89 transgenic female NSG mice were injected s.c. with $2.5×10^6$ cells in 150 µL and tumor outgrowth was measured using a caliper (length × width × height) until tumor size reached 1500 mm³. In indicated experiments, mice were treated intraperitoneally (i.p.) thrice a week (starting from day 5) with indicated doses of IgG1 ch14.18, IgA3.0 ch14.18 or PBS as a control.

For the immunocompetent model, CD89 transgenic male C57BL/6 mice were injected i.p. with $5×10^5$ luc2-transduced 9464D-GD2 cells. From day 6 onward, mice were injected i.p. twice per week with PBS or indicated doses of IgA3.0 ch14.18. To quantify tumor outgrowth, mice were injected i.p. with 100 µl of 25 mg/mL luciferin (Promega). 10 min after injection, mice were subjected to bioluminescence imaging at autoexposure settings (PhotonImager, MIlabs).

Indium-111 labeling and SPECT/CT scans

IgG1 and IgA3.0 ch14.18 (500 µg, 1 mg/mL) were attached to a Bn-DTPA metal linker (Macrocyclics) and Bn-DTPA-antibodies were labeled with Indium-111 ($^{111}InCl_3$, activity of 370 MBq/mL, Mallinckrodt). Fractions containing ^{111}In-labeled antibody were collected. Purity was assessed by running samples with 0.1 M citrate buffer on an iTLC (instant Thin-Layer Chromatography) strip (Agilent) followed by radio-TLC scanning. Purity for both IgA3.0 and IgG1 was over 97% (online supplemental figure 5D). CD89 transgenic NSG mice with s.c. IMR32 tumors (±1200 mm³) were injected i.v. with either 1.6

MBq ^{111}In-labeled IgG1 or 3.2 MBq ^{111}In-labeled IgA3.0 ch14.18. After 24 hours and 48 hours single-photon emission computed tomography (SPECT)/CT scans were acquired as specified in the online supplemental file 1.

Mouse tissue collection and flow cytometric analysis

Peritoneal lavage was performed using 6 mL PBS containing 5 mM EDTA. Mouse tumors and spleens were carefully excised and collected in ice cold PBS. Mouse blood was collected in lithium-heparin tubes (Sarstedt) and erythrocyte lysis was performed twice at room temperature for 5 min. Tumors were cut and digested using the mouse tumor dissociation kit from Miltenyi. Up to 1 g of tumor tissue was transferred to C tubes (Miltenyi) containing enzyme mix (DMEM culture medium, 100 µL Enzyme D, 50 µL Enzyme R, and 10 µL Enzyme A) and the 37C_m_TDK_1 program was run on a gentleMACS Octo Dissociator. Dissociated tumor cells and spleens were put through a 100 µm cell strainer and together with mouse blood stained (see online supplemental table 3) for analysis on the LSRFortessa. Tumor and spleen opsonization and IgA3.0 Fc-binding on neutrophils was determined by staining with goat F(ab')2 anti-human IgA-PE (1:200, SouthernBiotech).

Statistics and software

Statistical analysis was conducted using GraphPad Prism software (V.9.3.0). Means are represented with SD values, unless specified otherwise. Specific statistical analyses are indicated per experiment. All analyses were two-tailed and when post-hoc testing was required, we applied Tukey's post-hoc test. Significance is indicated by *p<0.05, **p<0.01, ***p<0.001 and ****p<0.0001. Flow cytometry analysis was done in FlowJo (Tree Star).

RESULTS

Characterization of IgA3.0 ch14.18 target (Fab) and Fc binding

After production and purification of the antibody variants, we assessed their binding to endogenous GD2 by immobilizing the antibodies to a plate and allowing neuroblastoma cells with high (IMR32, Lan-5), low (SKNFI) and no (GIMEN) GD2 expression to bind (online supplemental figure 1A). We chose this set-up instead of more conventional FACS-based assays, since it is less susceptible to variation induced by antibody internalization and GD2/antibody shedding. All antibody isotypes displayed similar binding to GD2, since neuroblastoma cells detached at similar rates on washing (figure 1B). Neuroblastoma cells with higher GD2 expression (IMR32, Lan-5) detached slower than cells with low expression (SKNFI) and GD2-negative GIMEN cells did not bind to the antibody variants at all, indicating antibody binding is dependent on GD2 expression.

Next to target binding, we investigated Fc-mediated, monomeric (cytophilic) binding to CD89 by incubating CD89-expressing Ba/F3 cells, CD89 transgenic murine neutrophils and human PMN with the ch14.18 variants.

Interestingly, at various concentrations IgA3.0 ch14.18 showed increased binding to CD89 on these three cell types compared with IgA1 and IgA2 (figure 1C–E, online supplemental figure 1B–E). IgG1 ch14.18 was taken along as a reference, but was not analyzed since binding is mediated by Fc gamma receptors (FcγRs). IgA variants did not bind to murine neutrophils from non-transgenic mice (online supplemental figure 1B), indicating that binding is CD89-specific. We studied complexed IgA binding by incubating calcein-labeled murine neutrophils and Ba/F3-CD89 cells on plates coated with antibody complexes. Though complexed IgA3.0 binding to Ba/F3-CD89 cells was slightly decreased compared with IgA1 and IgA2, no major differences in binding to CD89 transgenic neutrophils was observed (figure 1F,G, online supplemental figure 1F–H).

IgA3.0-mediated ADCC is similar to IgA1 and superior to IgA2

To study the influence of IgA3.0 mutations on ADCC induction, we performed ^{51}Cr release assays using multiple neuroblastoma cell lines with both low (SKNAS, SKNFI) and high (IMR32) GD2 expression (online supplemental figure1A). As expected, IgG1 ch14.18 induced more ADCC of SKNAS and IMR32 cells than IgA with PBMC as effector cells (figure 2A), but all IgA variants induced better ADCC with PMN as effector cells (figure 2B). Though no differences were observed between IgA variants when PBMC were used as effector cells, IgA1 and IgA3.0 outperform IgA2 in ADCC assays with PMN (figure 2B), suggesting that the optimized IgA3.0 format improved ADCC. However, in WBL ADCC assays all ch14.18 antibodies performed similarly, only at lower antibody concentrations IgA1 and IgA3.0 performed slightly better than IgA2 (figure 2C). ADCC induction was dependent on GD2-expression, since GD2-negative cell lines (9464D, GIMEN) were not lysed (online supplemental figure 2A).

In order to explore a non-human primate model for preclinical testing in the future, we measured CD89 expression and ADCC in cynomolgus monkeys (*Macaca fascicularis*). We found that cynomolgus monkeys express high levels of CD89 on granulocytes and lower levels on monocytes, corresponding to the human expression profile (figure 2D). IgA3.0 ch14.18 induced killing of IMR32 cells by PMN from all cynomolgus donors tested and the percentage of tumor cell lysis was comparable to human PMN (figure 2E, online supplemental figure 2B).

Furthermore, we tested whether neuroblastoma patient-derived effector cells can kill IMR32 tumor cells with IgA3.0 ch14.18, since immune cells in cancer patients can be exhausted and/or dysfunctional. Interestingly, neuroblastoma patient-derived PMN killed IMR32 cells efficiently when stimulated with IgA3.0 ch14.18 (figure 2F, online supplemental figure 2C). However, IgG-mediated killing with patient PBMC was severely reduced compared with healthy donor PBMC, with both anti-GD2 and anti-EGFR IgG antibodies (figure 2G, online supplemental figure 2C). Relative
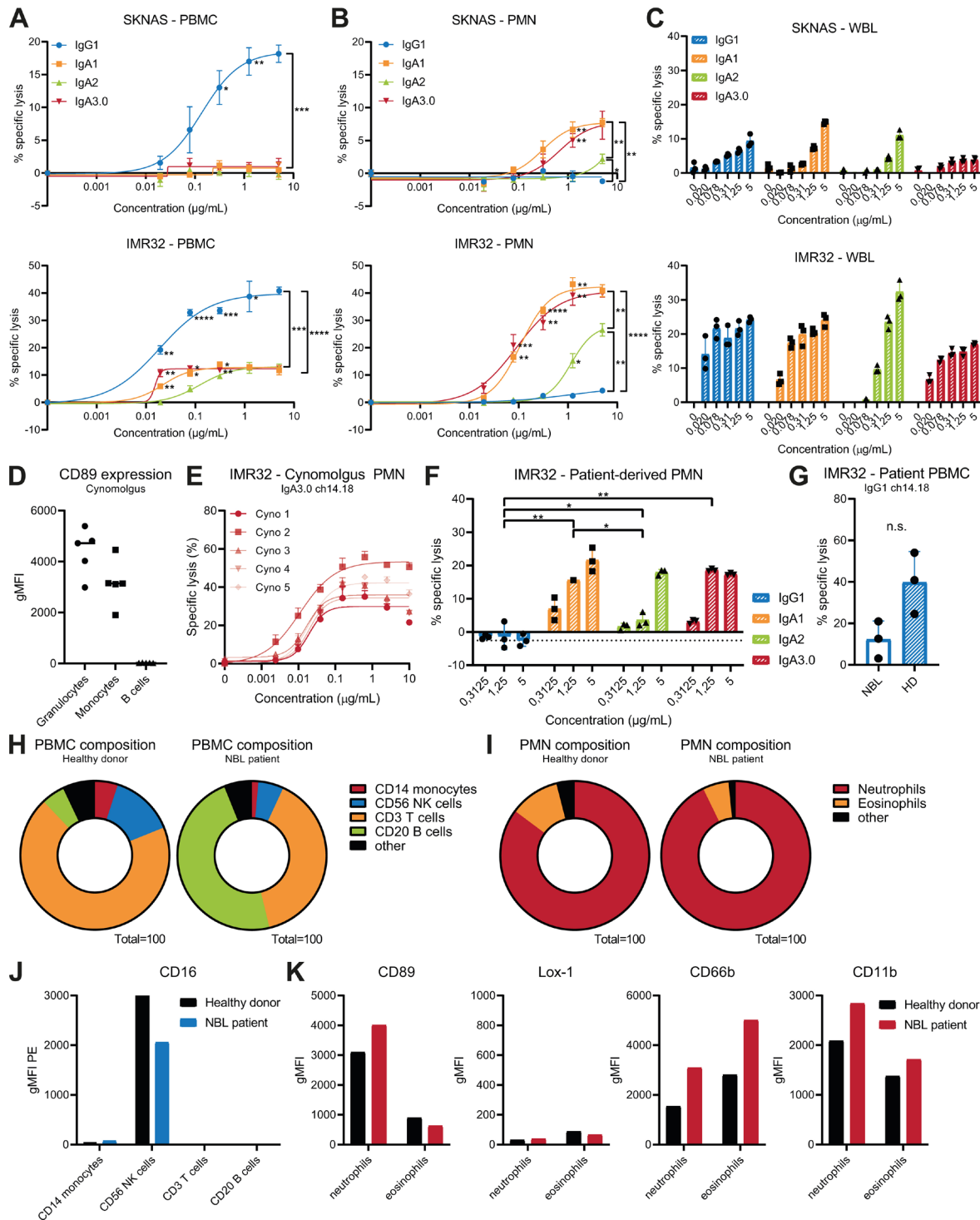
Figure 2 IgA3.0-mediated ADCC is similar to IgA1 and superior to IgA2. Efficiency of antibodies in inducing ADCC against neuroblastoma target cells in ^{51}Cr-release assays with either (A) PBMC, (B) PMN or (C) WBL as effector cells. ADCCs were compared using two-way ANOVA. (D) Flow cytometry analysis of CD89 expression on cynomolgus leukocytes. (E) ^{51}Cr-release assays with cynomolgus PMN as effector cells against IMR32 cells. (F) ^{51}Cr-release assays with neuroblastoma patient PMN against IMR32 cells. Dotted line is the no antibody background. Means were compared using two-way ANOVA. (G) ^{51}Cr-release assays with neuroblastoma patient PBMC and healthy donor PBMC from three different donors/patients against IMR32 cells. Means were compared using a paired t-test. (H) PBMC and (I) PMN composition in healthy donor and neuroblastoma patient blood. (J) CD16 expression in healthy donor and neuroblastoma patient blood. (K) Expression of neutrophil activation markers in healthy donor and neuroblastoma patient blood. Data as shown are mean±SD, n=3 for all ADCC assays. Healthy donor and patient ADCCs were performed three times and cynomolgus ADCC once. *p<0.05, **p<0.01, ***p<0.001 and ****p<0.0001. ADCC, antibody-dependent cell-mediated cytotoxicity; ANOVA, analysis of variance; gMFI, geometric mean fluorescence intensity; NBL, neuroblastoma; NK, natural killer; PBMC, peripheral blood mononuclear cells; PE, phycoerythrin; PMN, polymorphonuclear leukocytes; WBL, whole blood leukocytes.

quantification showed that NK cells and monocytes were reduced, though total number of PBMC and PMN was similar between patients with neuroblastoma and healthy donors (figure 2H,I). Additionally, CD16 (FcγRIIIa) expression on NK cells was reduced in patients with neuroblastoma (figure 2J). On the other hand, PMN from patients with neuroblastoma expressed higher levels of CD89, CD66b and CD11b (figure 2K), reflecting a more activated phenotype. Therefore, considering the immune cell composition of patients with neuroblastoma, IgA3.0 ch14.18

immunotherapy might be favorable compared with IgG1 ch14.18.

IgA3.0 ch14.18 induces ADCP with both M0, M1 and immunosuppressive M2 mφ

ADCP is considered a major mode of action for IgG antibodies, but since monocytes and macrophages also express CD89 to some extent,[37] IgA-mediated phagocytosis could contribute to the antitumor effect of IgA3.0 ch14.18. Therefore we established ADCP assays in which macrophages (mφ) become fluorescent after engulfing
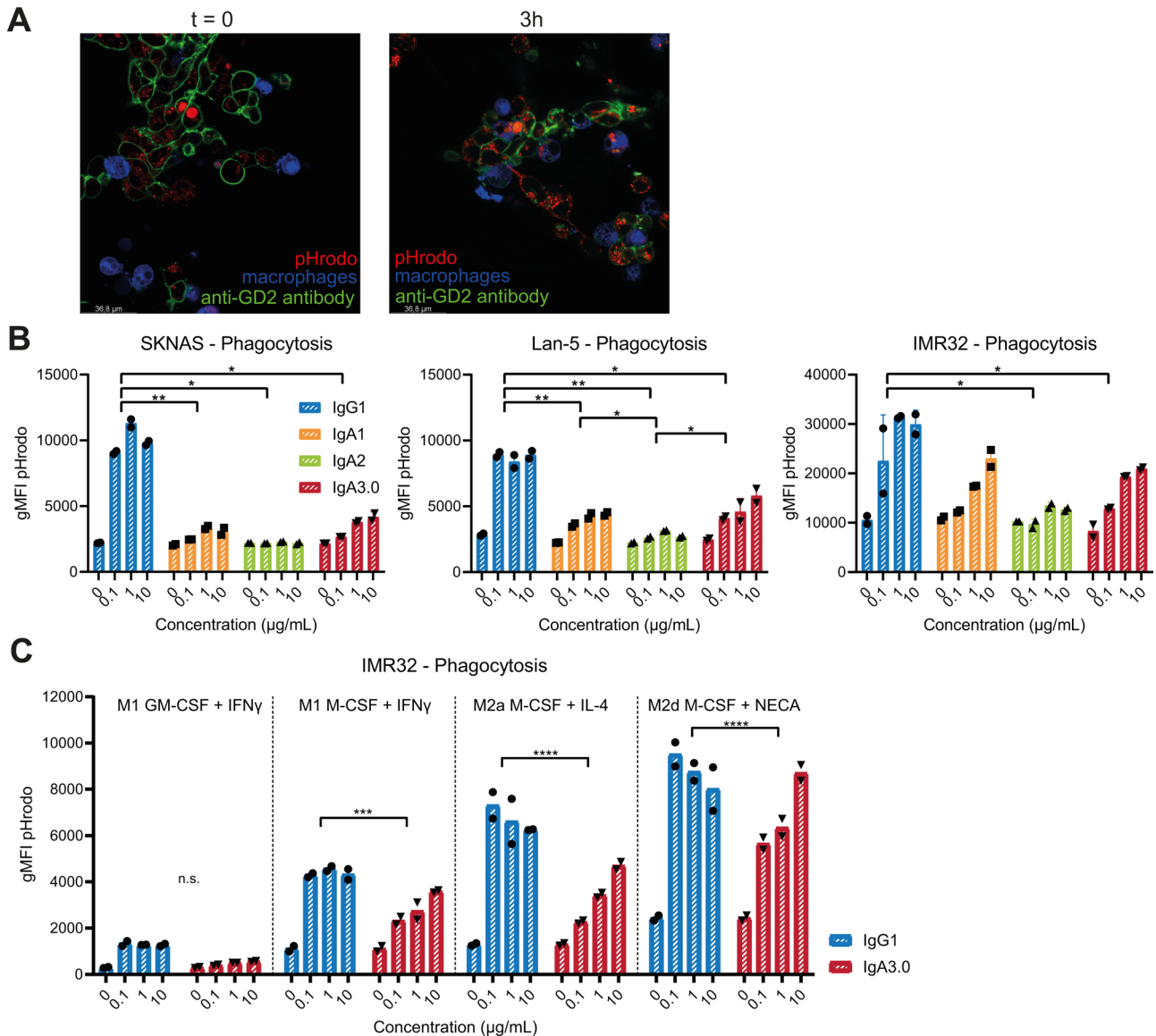

Figure 3 IgA3.0 ch14.18 induces ADCP in both M0, M1 and M2 macrophages. (A) Confocal images before and after 3 hours incubation of pHrodo-labeled target cells with FITC-labeled anti-GD2 antibody and CTV-labeled macrophages. (B) The efficiency of antibodies in inducing phagocytosis against pHrodo-labeled human neuroblastoma target cells by M-CSF-differentiated, monocyte-derived macrophages as effector cells. (C) The efficiency of antibodies in inducing phagocytosis by macrophages polarized with IFN-γ, IL-4, or 5 μM NECA. Antibodies were compared using two-way ANOVA. Data as shown are means, n=2. Phagocytosis assays were performed twice. *p<0.05, **p<0.01, ***p<0.001 and ****p<0.0001. ADCP, antibody-dependent cell-mediated phagocytosis; ANOVA, analysis of variance; CTV, CellTrace Violet; FITC, fluorescein isothiocyanate; GM-CSF, granulocyte-macrophage colony-stimulating factor; gMFI, geometric mean fluorescence intensity; IFN, interferon; IL, interleukin; M-CSF, macrophage colony-stimulating factor.

pHrodo-labeled target cells that are opsonized with anti-GD2 antibody (figure 3A). As in ADCC, IgA1 and IgA3.0 antibodies slightly outperformed IgA2 in inducing phagocytosis of IMR32, Lan-5 and SKNAS cells by M-CSF differentiated M0 mφ (figure 3B). Again, IMR32 and Lan-5 cells are phagocytosed more efficiently compared with SKNAS cells. SKNFI cells were poorly phagocytosed on both IgG1 or IgA3.0 ch14.18 stimulation (online supplemental figure 2E). Generally, cells that are susceptible to IgG-induced phagocytosis are susceptible to IgA-mediated phagocytosis as well.

In the tumor microenvironment however, often more activated and/or polarized macrophages are present. Therefore, we investigated whether M1 mφ (induced by IFN-γ), M2a mφ (induced by IL-4) and M2d mφ (induced by an adenosine receptor agonist, NECA)[38] are able to kill neuroblastoma cells with IgA antibodies as well. Surprisingly, IgA3.0 ch14.18 induced relatively more tumor cell lysis with M2a mφ and M2d mφ compared with M1 mφ (figure 3C), though it must be noted that M2d mφ were already killing more tumor cells spontaneously without antibody stimulation (0 µg/mL condition). Additionally, GM-CSF differentiated macrophages phagocytosed tumor cells less well compared with macrophages differentiated by M-CSF.

Protein stability is improved by IgA3.0 mutations

To evaluate whether IgA3.0 mutations have improved antibody stability, we performed Sypro Orange thermal shift assays. In general, the IgA3.0 isotype displays a higher melting temperature relative to all other isotypes as observed for antibodies targeting CD47, CD20, Her2/neu and EGFR (online supplemental figure 3A). Similar to these antibodies against other targets, IgG1 ch14.18 started dissociating at lower temperatures compared with all ch14.18 IgA variants (figure 4A). From all ch14.18 IgA variants, IgA2 has the lowest melting temperature (figure 4B), although the difference is rather small. These results combined suggest that IgA3.0 mutations increase antibody stability, although of less significance in the ch14.18 format. Additionally, we investigated whether different production cell lines (HEK293F, ExpiCHO-S and CHO K1) influence protein stability. As no differences in Tm values were observed, the type of production cell did not impact antibody stability (figure 4B,C).

N-glycosylation pattern on IgA3.0 ch14.18 is favorable for its half-life

We further characterized the IgA3.0 ch14.18 molecule by performing mass spectrometry to study the *N*-linked glycosylation profile. Mass spectrometry confirmed that *N*-linked glycosylation on IgA3.0 antibodies was silenced at all sites except for the N20 site in the CH2 domain and therefore IgA3.0 has less glycosylation in general compared with IgA1 and IgA2. As in IgG antibodies, most *N*-linked glycan structures present on the IgA variants were complex, diantennary glycans (figure 4D, online supplemental figure 4) except for the N135 site in the CH3 domain of IgA2, where some

tri-antennary or tetra-antennary glycans were found as well. Core fucosylation is present on IgG1, IgA1 and IgA2 antibodies, but since core fucosylation is almost absent at the N20 site, IgA3.0 antibodies are practically devoid of core fucosylation (figure 4E).

Interestingly, when comparing glycosylation at the N20 site between IgA2 and IgA3.0 produced in HEK293F cells, sialic acids are relatively increased in IgA3.0 (figure 4F,G). However, the presence of terminal sialylation appears to be dependent on the production host cell line, since sialylation of IgA3.0 ch14.18 produced in CHO-K1 or Expi-CHO-S is not increased (figure 4H,I). Since high levels of sialylation on IgA antibodies limit degradation via the ASGPR, this glycosylation pattern could be beneficial for the half-life of IgA3.0. Similarly, IgA3.0 ch14.18 produced in HEK293F contains less terminal mannose structures on N20 when compared with IgA2, but IgA3.0 ch14.18 produced in CHO-K1 or Expi-CHO-S systems have similar amounts of terminal mannoses (figure 4F and H, online supplemental figure 4). IgA antibodies with reduced uncapped mannoses could have a longer half-life as well, since proteins containing glycans with terminal mannoses are susceptible for scavenging via the mannose receptor. Overall, IgA3.0 mutations decrease the absolute amount of glycosylation and production of IgA3.0 ch14.18 in HEK293F cells results in a more mature glycosylation pattern containing less terminal mannose and galactose residues, rendering IgA3.0 ch14.18 less susceptible to degradation via glycan receptors.

IgA3.0 ch14.18 serum half-life is prolonged compared with IgA1 and IgA2

To assess whether this favorable glycosylation pattern indeed correlates with increased half-life in vivo, we performed PK studies in CD89 transgenic Balb/c and NSG mice. As described previously,[39] we found that IgG ch14.18 has a shorter half-life in NSG mice compared with Balb/c mice (figure 5A,B). However, half-lives of IgA antibody variants are similar between these two mouse strains (figure 5A,B). Next, we focused on the distribution phase of IgA antibodies and observed that whereas IgA1 and IgA2 serum concentrations decline considerably in the first hour, IgA3.0 antibody concentrations remain high, similar to IgG1 (figure 5C). The significantly higher cumulative antibody exposure of IgA3.0 (figure 5D) can be attributed to this improved distribution phase, since no major changes in half-life values between IgA variants were observed in the elimination phase (figure 5A,B). These PK data strongly support the hypothesis that the decreased and improved glycosylation of IgA3.0 ch14.18 rescues the molecule from rapid glycan-mediated uptake via the ASGPR and mannose receptor.

Additionally, serum concentrations of IgA3.0 ch14.18 produced in Expi-CHO-S declined faster compared with HEK293F-produced IgA3.0, though not significantly. (figure 5E) This corresponds with the favorable glycosylation pattern of HEK293F-produced IgA3.0 ch14.18 as described earlier. We have observed similar findings for
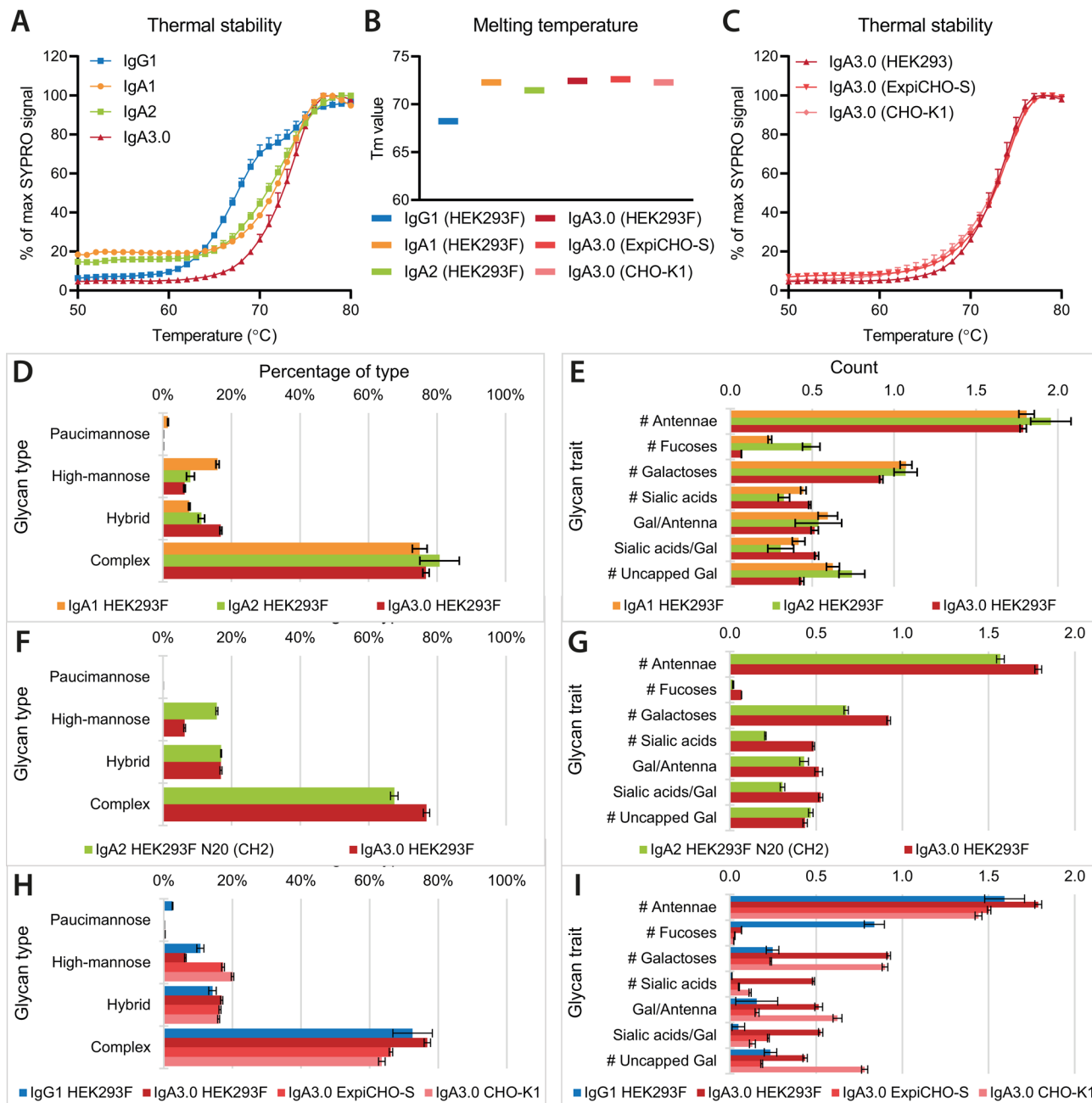
Figure 4 IgA3.0 mutations result in improved stability and in a favorable glycosylation pattern. (A) Sypro orange thermal shift assays for ch14.18 antibody variants. (B) Tm values as calculated by transforming temperature values to log(10) followed by non-linear regression on the transformed data from thermal shift assays. (C) Sypro orange thermal shift assays for ch14.18 IgA3.0 produced in different production cell lines. Mass spectrometry analysis (D, E) of overall glycosylation in IgA ch14.18 variants, (F, G) of glycosylation at the N20 site in the CH2 domain and (H, I) of glycosylation of IgA3.0 ch14.18 produced in HEK293F, Expi-CHO-S or CHO-K1. Data as shown are mean±SD, n=3.

IgA3.0 antibodies targeting for example CD20, (online supplemental figure 5A) but it is possible that HEK293F cells are not the best production cell line for IgA antibodies against all targets. These data underscore the importance of choosing the best cell line for clinical batch production.

IgA3.0 ch14.18 penetrates and opsonizes IMR32 neuroblastoma tumors in vivo

Next, we studied the biodistribution of IgA3.0 ch14.18 in vivo to confirm that it is able to reach and opsonize neuroblastoma tumors. First, we injected 25 mg/kg IgA3.0 ch14.18 to evaluate whether the small increase in monomeric binding observed in vitro would result in binding to CD89 in vivo. Neutrophils from CD89 transgenic mice did not have bound IgA3.0 ch14.18 after 24 hours. However, when we incubated these neutrophils
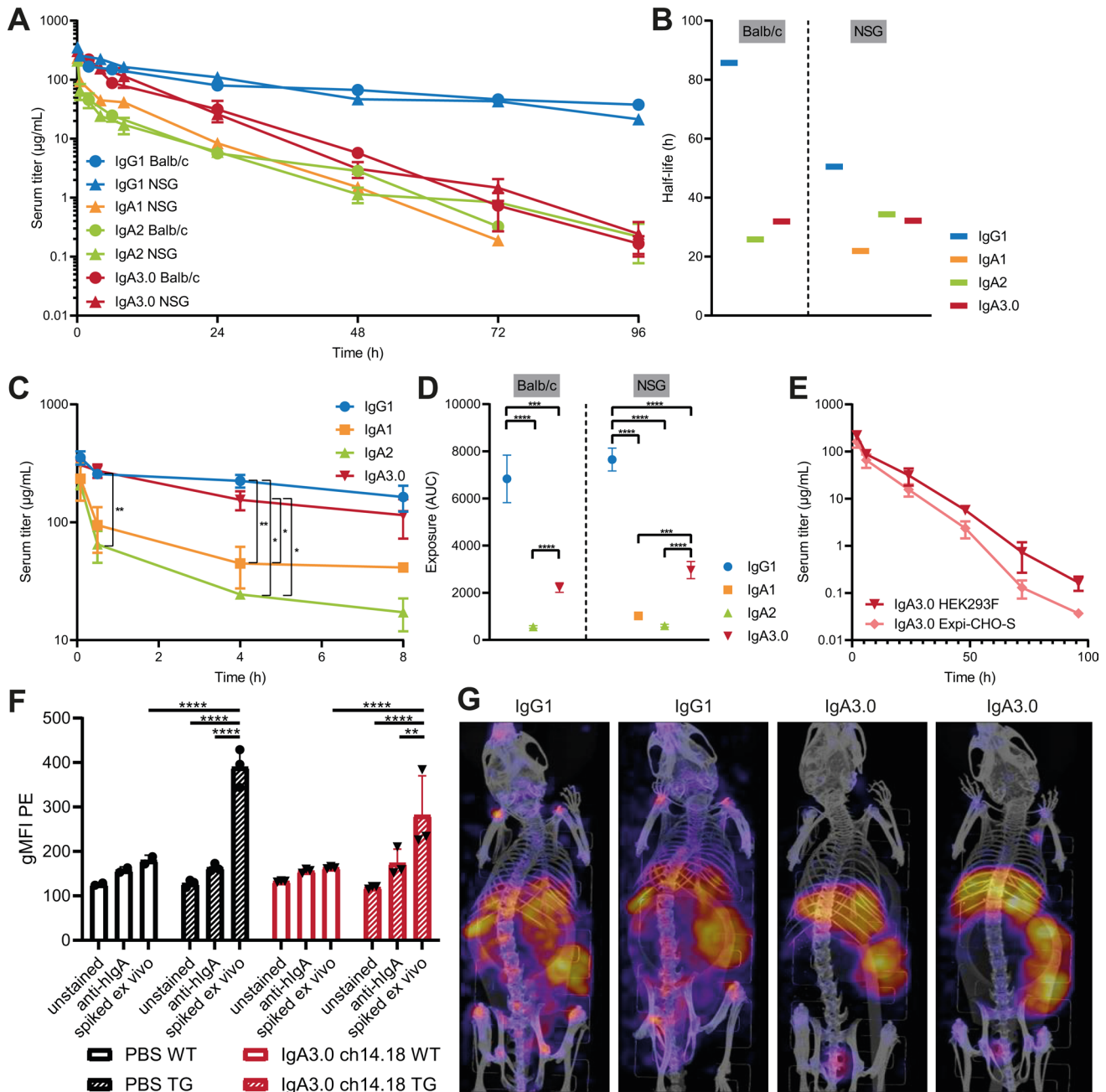
Figure 5 PK and biodistribution studies for ch14.18 antibody isotypes in Balb/c and NSG mice. (A) CD89 transgenic Balb/c and NSG mice were injected i.v. with 5 mg/kg antibody solution (HEK293F produced) and serum concentrations over time were determined using ELISA on blood samples collected from the submandibular vein. (B) Half-life values calculated for the elimination phase (24–96 hour). (C) Distribution phase of the ch14.18 antibody variants. A mixed models analysis was performed on 30 min, 4-hour and 8-hour time points. (D) Cumulative antibody exposure in NSG mice as calculated by AUC analysis. AUC was compared with one-way ANOVA analysis. (E) Serum concentrations in Balb/c mice over time after i.v. injection of 5 mg/kg HEK293F produced and Expi-CHO-S produced IgA3.0 ch14.18. Means were compared using a mixed models analysis. (F) Circulating neutrophils of mice treated with PBS or 25 mg/kg IgA3.0 ch14.18 were isolated, incubated ex vivo with IgA3.0 ch14.18 and/or stained with PE-labeled anti-hIgA antibodies to determine monomeric CD89 binding. (G) Overlay of SPECT/CT scans displaying the biodistribution after 24 hours of ^{111}In-labeled ch14.18 antibodies in CD89 transgenic mice bearing an IMR32 neuroblastoma tumor. Data as shown are mean±SD, n=3 for PK studies and monomeric binding, n=2 for biodistribution scans. * as p<0.05, ** as p<0.01, *** as p<0.001 and **** as p<0.0001. AUC, area under the curve; CHO, Chinese hamster ovarian cells; gMFI, geometric mean fluorescence intensity; HEK293F cells, human293 cells; NSG, NODSCID gamma mice; PBS, phosphate-buffered saline, PE, phycoerythrin; TG, transgenic mice; WT, wild type mice.

with IgA3.0 ch14.18 ex vivo, it was able to bind to CD89 on neutrophils.

Second, we injected CD89 transgenic IMR32 tumor-bearing mice with either IgA3.0 or IgG1 ch14.18 or an isotype control (palivizumab) and measured tumor opsonization after 24 hours. Both IgA3.0 and IgG1 ch14.18 opsonized neuroblastoma tumors to a large extent, since tumor single cell suspensions spiked with antibodies ex vivo (at saturating concentrations) showed comparable levels of opsonization (online supplemental figure 5B). Some background staining for the isotype control was observed, which is probably binding to non-tumor cells expressing FcγRs, since IgG antibodies bound splenocytes as well (online supplemental figure 5C). To confirm our findings, we performed biodistribution SPECT/CT scans of mice injected with ^{111}-In-labeled IgG1 or IgA3.0 ch14.18. Both IgG1 and IgA3.0 specifically concentrated in the tumor and reached the tumor center (figure 5F,G). Especially IgA3.0 was retained in the tumor after 48 hours. Additionally, high signal was observed in the liver (catabolism) and to a lower extent in the bladder (excretion). In conclusion, IgA3.0 ch14.18 reaches and opsonizes IMR32 neuroblastoma tumors in vivo at least as well as IgG1 ch14.18.

Subcutaneous IMR32 tumor outgrowth in NSG mice is halted by IgA3.0 ch14.18

Assessing the in vivo efficacy of IgA antibodies can be rather challenging, since mice do not naturally express CD89 and mice have a much lower number of neutrophils (~10% of circulating leukocytes) compared with humans (~50–70%). On top of that, murine neutrophils are less effective in killing tumor cells upon IgA3.0 treatment compared to human neutrophils (figure 6A). Nevertheless, we developed a human xenograft and an immunocompetent model in mice transgenically expressing human CD89 to evaluate the in vivo efficacy of IgA3.0 ch14.18.

To establish a human xenograft model, we injected CD89 transgenic NSG mice s.c. with IMR32 neuroblastoma tumor cells and subsequently treated with different doses of IgA3.0 ch14.18 starting from day 5. Doses were based on literature describing dinutuximab treatment in mouse tumor models[40–42] and corrected for the difference in half-life. All doses showed small treatment effects, but only the highest dose (60 mg/kg) of IgA3.0 ch14.18 impeded tumor growth (figure 6B) and prolonged tumor-specific survival of IMR32 tumor-bearing mice significantly (figure 6C). All doses resulted in tumor opsonization with IgA3.0 ch14.18 (figure 6D) and additionally, IgA3.0 was binding to intratumoral neutrophils, which increased along with higher doses administered (figure 6E). Detection of CD89 on tumor-infiltrating neutrophils and monocytes was reduced (online supplemental figure 6 and 7A), suggesting Fc-mediated binding of IgA3.0 ch14.18 to CD89 hindering binding of detection antibodies.

Flow cytometric analysis of immune cells in the tumor microenvironment showed no attraction of myeloid cells, such as neutrophils, monocytes and macrophages after IgA3.0 therapy (figure 6F). Blood and spleen immune cell composition remained unaffected as well (online supplemental figure 7B). Considering the relative absence of myeloid cells and the small therapeutic effect it appears that murine myeloid cells are only minimally activated to kill tumor cells as was observed in ex vivo ADCC assays.

For comparing efficacy between IgA3.0 and IgG ch14.18, similar serum levels were used as comparators rather than equal dosages, because of the substantial difference in half-life. When we compared IgA3.0 ch14.18 efficacy with an historical experiment with similar IgG1 ch14.18 serum concentrations (online supplemental figure 7C), we observed that IgA3.0 ch14.18 has a similar or slightly better therapeutic effect compared with IgG1 (online supplemental figure 7D–E).

IgA3.0 ch14.18 is reducing outgrowth of intraperitoneal 9464D-GD2 tumors

Next, we assessed the efficacy of IgA3.0 ch14.18 in an immunocompetent mouse model by injecting luciferase-expressing 9464D-GD2 cells i.p. in CD89 expressing C57BL/6 mice. Treatment started on day 7 and mice received IgA3.0 ch14.18 or PBS treatment i.p. twice a week. Doses were decreased compared with the s.c. IMR32 model, since therapy is injected close to the tumor site. Both the 10 mg/kg and the 25 mg/kg dose induced a significant delay of tumor outgrowth and prolonged survival and even the lowest dose (2.5 mg/kg) exhibits a minor effect (figure 7A,B, online supplemental figure 8A). As in the IMR32 tumor model, there is no influx of myeloid cells in the peritoneum or tumor microenvironment after treatment (figure 7C,D, online supplemental figure 9). If there is any effect, we observed a minor reduction of neutrophils and monocytes compared with the PBS control tumors, but most differences are not significant. No changes of myeloid cells in the blood (online supplemental figure 8B) or T cells numbers (online supplemental figure 8C) were noticed either. However, similar to the IMR32 tumors, lower levels of CD89 were detected on intratumoral and intraperitoneal myeloid cells, especially in the highest dosed group (online supplemental figure 8D). Combining these results, it is likely that the therapeutic efficacy of IgA3.0 ch14.18 is executed mostly by tumor-resident immune cells. This hypothesis would explain that IgA3.0 ch14.18 is more effective in the 9464D-GD2 model as well, since these tumors have roughly 10 times more myeloid cells infiltrating the tumor (figures 6F and 7C).

Finally, as described for the IMR32 model, we compared efficacy of IgA3.0 ch14.18 with IgG1 ch14.18 in the 9464D-GD2 model historically, based on similar serum levels (online supplemental figure 8E). Again, we observed that IgA3.0 ch14.18 has a similar or slightly better therapeutic effect compared with IgG1 (online supplemental figure 8F and G).
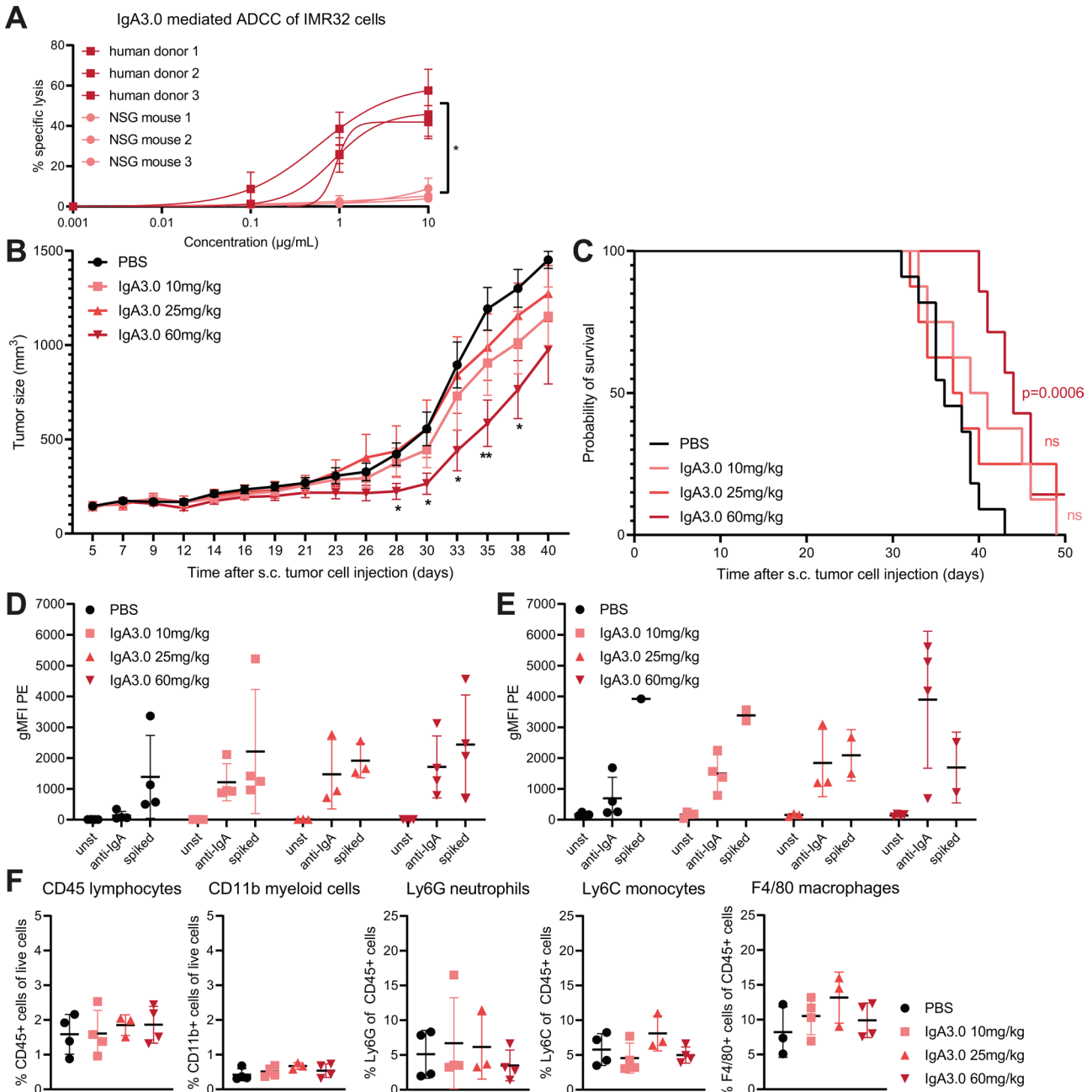
Figure 6 Subcutaneous IMR32 tumor outgrowth in NSG mice is halted by IgA3.0 ch14.18. (A) Comparison of human PMN and NSG mouse neutrophil ADCC against neuroblastoma target cells with IgA3.0 ch14.18 in ^{51}Cr-release assays. (B) NSG mice were injected s.c. with $2.5×10^6$ IMR32 tumor cells and treated thrice a week with PBS or increasing dosages of IgA3.0 ch14.18 from day 5 onwards. Tumor outgrowth was measured thrice a week until the end point (tumor size of 1500 mm³) was reached. Tumor sizes were compared using a two-way ANOVA. Asterisks indicate significance compared with PBS control group. (C) Kaplan-Meier curve of tumor-specific survival. Log-rank test for trend p=0.0092. PBS/ IgA3.0 10 mg/kg ns, PBS/IgA3.0 25 mg/kg ns, PBS 60 mg/kg p=0.0006 (log-rank test). Single-cell suspensions derived from IMR32 tumors were stained with anti-hIgA antibodies to determine (D) tumor cell opsonization and (E) Fc-mediated, cytophilic binding to intratumoral neutrophils by flow cytometry. (F) Immune cell composition of IMR32 tumors at the end point was determined by flow cytometry on tumor single cell suspension. PBS and treatment groups were compared with one-way ANOVA. Data as shown are mean±SEM for tumor measurements and mean±SD for flow cytometry data. N=10 for PBS, n=8 for 10 mg/kg and 25 mg/kg and n=7 for 60 mg/kg. *p<0.05, **p<0.01, ***p<0.001 and ***p<0.0001. ADCC, antibody-dependent cell-mediated cytotoxicity; ANOVA, analysis of variance; gMFI, geometric mean fluorescence intensity; NSG, NOD SCID gamma mice; PBS, phosphate-buffered saline; PE, phycoerythrin; PMN, polymorphonuclear leukocytes; s.c., subcutaneous; Unst, unstained.
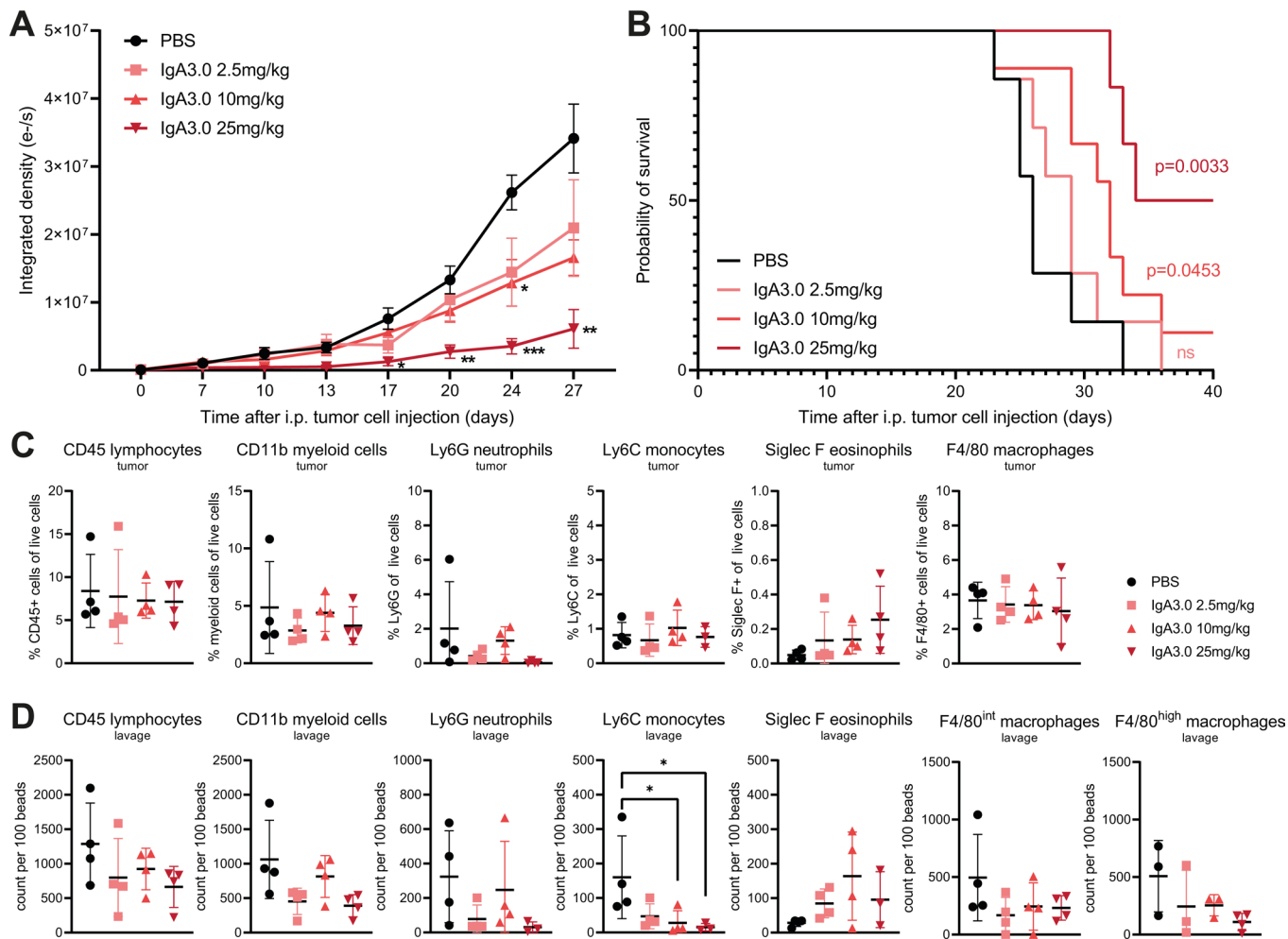
Figure 7 IgA3.0 ch14.18 is reducing outgrowth of intraperitoneal 9464D-GD2 tumors. Tumor outgrowth was measured twice a week until the end point (BLI signal of 30×10^{6}) was reached. (A) Tumor sizes were compared using a mixed-effects model analysis. Asterisks indicate significance compared with PBS control group. (B) Kaplan-Meier curve of tumor-specific survival. Log-rank test for trend p=0.0002. PBS/ IgA3.0 2.5 mg/kg ns, PBS/IgA3.0 10 mg/kg 0.0453, PBS 25 mg/kg p=0.0033 (log-rank test). Immune cell composition of (C) 9464D-GD2 tumors (D) and peritoneal lavage at the end point was determined by flow cytometry analysis on single cell suspension. PBS and treatment groups were compared with one-way ANOVA. Data as shown are mean±SEM for tumor measurements and mean±SD for flow cytometry data. N=7 for PBS, n=8 for 2.5 mg/kg, n=9 for 10 mg/kg and n=6 for 60 mg/kg. *p<0.05, **p<0.01, ***p<0.001 and ****p<0.0001. ANOVA, analysis of variance; BLI, bioluminescence imaging; i.p., intraperitoneal; PBS, phosphate-buffered saline.

DISCUSSION

Previously, it was demonstrated that IgA1 ch14.18 antibodies are effective against neuroblastoma models in vitro and in vivo and that they do not induce neuropathic pain, whereas IgG1 ch14.18 does.[13] In the present study, we engineered IgA2m(1) into a novel IgA3.0 molecule, which resulted in similar binding and tumor killing, but increased stability, improved glycosylation and elongated half-life compared with non-engineered IgA1 and IgA2. Additionally, we have shown that IgA3.0 ch14.18 penetrates neuroblastoma tumors in vivo and reduces tumor outgrowth in both immunocompetent and human xenograft mouse tumor models.

Though target binding is similar for all ch14.18 isotypes, we observed a small increase in monomeric binding of the IgA3.0 ch14.18 Fc tail to CD89. In the past, no increased Fc tail affinity was found for antibodies in the IgA2.0

format.[32] Since the only difference between the IgA2.0 and the IgA3.0 molecule is the removal of the tail piece, the tail piece (including the N-glycan N135) may be critically involved in binding to CD89. However, we did not compare Fc tail affinity of IgA2.0 and IgA3.0 head-to-head in the ch14.18 format. Hence these results should be validated in the future, for example, with surface plasmon resonance or ligand tracer experiments. Furthermore, it would be of interest to know whether only the glycan structure at N135 is responsible for differences in affinity for CD89, or whether the whole tail piece is involved. Göritzer and colleagues studied N-glycosylation by producing IgA antibodies in *Nicotiana benthamiana* plants lacking the enzymes synthesizing N-glycans.[43 44] They did not observe an increase in Fc tail affinity in IgA molecules lacking N-glycans, suggesting that deletion of the entire tail piece is responsible for the small increase in Fc affinity

that we found. Increased Fc tail affinity could theoretically be problematic for tumor penetration of antibodies, by spontaneously binding to CD89-expressing leukocytes in the circulation. However, we observed clear opsonization and penetration of neuroblastoma tumors in CD89 transgenic mice by IgA3.0 ch14.18 (figure 5F). Since affinity for complexed IgA was not increased and monomeric antibody binding does not crosslink the FcαRI, we do not expect neutrophil activation in the circulation. No adverse effects were observed in mice exposed to high doses of IgA (60 mg/kg), suggesting that neutrophils are not randomly activated in vivo.

In the present study, we did observe that IgA3.0 ch14.18 increased PMN ADCC and macrophage ADCP (but not WBL ADCC) compared with IgA2, which could be caused by the changes in the glycosylation pattern and/or tail piece deletion. Additionally, we detected a modest increase in protein stability, which is known to be affected by glycosylation as well.[45 46] Currently, there is limited insight in the impact of glycosylation patterns on the Fc-mediated effector function of IgA antibodies, although it has been described that removal of sialic acids in IgA1 results in more pro-inflammatory function.[47] Therefore, it would be interesting to study the impact of each of the IgA3.0 mutations and accompanying changes in glycosylation on effector functions such as ADCC, neutrophil extracellular trap formation and cytokine secretion by neutrophils and other myeloid cells.

Next, we observed a more mature, terminally sialylated glycosylation pattern on IgA3.0 ch14.18 at the N20 site corresponding to an increased half-life in mice, but only when antibodies were produced in HEK293F cells. However, currently Chinese hamster ovarian cells (CHO) cells are the most opted choice for production of clinical-grade antibodies. If CHO cells will be used for clinical batch production, it should be considered to complement cells with, for example, glycan precursors[45] and/or enzymes responsible for the addition of terminal sialic acids.[46]

It is important to note that mouse half-life experiments are informative, but not directly translational to humans, since the IgA system is different in among others antibody repertoire development, pIgR-mediated transport, colostral IgA content, hepatobiliary transport and function.[48] Next to that, human IgG1 has an artificially long half-life in mice, because of its higher affinity for mouse FcRn compared with mouse IgG.[49] Finally, the half-life of IgG antibodies can differ between mouse models[39 50] which we observed as well in this study, as IgG1 ch14.18 had a shorter half-life in NSG compared with Balb/c mice. It has been described that the relatively fast clearance of IgG antibodies in NSG mice is dependent on FcγR-mediated clearance by myeloid cells, which can be prevented by pretreatment with hIVIg (human intravenous immunoglobulin).[39] We did not observe differences in half-life of IgA antibodies between NSG and Balb/c mice, implying that there is no similar mechanism for CD89-mediated clearance of IgA in NSG mice. For more accurate estimations of IgA3.0 ch14.18 half-life in humans, we could use cynomolgus monkeys. Since we found that they express CD89 similar to humans and perform comparable ADCC of IMR32 neuroblastoma cells, this animal model is well suitable for future toxicokinetic and PK studies.

Despite the short half-life of IgA in mice, we showed that IgA3.0 ch14.18 is significantly reducing tumor outgrowth in two different mouse tumor models, but it is not curative. It must be noted that both in our hands (online supplemental figure 7C–E) and in other studies (among which two studies on which Food and Drug Administration/European Medicines Agency approval was based) the effect of IgG1 ch14.18 in treating mouse neuroblastoma models is modest and high doses of IgG1 ch14.18 are required for a treatment effect.[40 51 52] IgG1 ch14.18 is proven effective in patients, hence this suggests that mouse neuroblastoma models are relatively hard to treat with anti-GD2 antibody therapy and that the therapeutic potential is underestimated in mouse experiments. As we demonstrated, this may be explained by the fact that murine neutrophils do not kill neuroblastoma cells as well as human neutrophils (figure 6A). Neutrophil numbers and activation might be lower due to the relative germ-free environment of laboratory mice as was demonstrated by Zhang et al.[53] However, neutrophils do seem to be required for the IgA3.0-mediated antitumor effect, since we observed a more significant treatment effect in the 9464D-GD2 tumors compared with the IMR32 tumors, which are relatively devoid of myeloid cells. Hence, it will be important to investigate whether neutrophil phenotype and/or tumor infiltration prior to treatment could be predictive for treatment response. Currently, we might also be underestimating the therapeutic potential of IgA3.0 relative to IgG1 ch14.18 in our in vitro assays, since most experiments were performed with healthy donor effector cells. However, we observed that patient PBMC (most importantly NK cells) are not as functional as PBMC from healthy individuals, while patient neutrophils are still efficiently killing tumor cells with IgA3.0 ch14.18.

With this study, we brought IgA3.0 ch14.18 immunotherapy forward to clinical application. Even though IgA antibody therapy is hard to study in mice due to the lack of CD89, development of mouse anti-human antibodies in long-term syngeneic models and low numbers of rather 'lazy' neutrophils, we demonstrated clear antitumor effects in vivo. Furthermore, considering that IgG1 ch14.18 is inducing less ADCC by neuroblastoma patient-derived effector cells than by healthy donor effector cells, we might underestimate the efficacy of IgA3.0 ch14.18 in this study. Still some outstanding questions will need to be investigated before clinical studies are initiated. For example, currently anti-GD2 immunotherapy is combined with the administration of GM-CSF, which is proven to enhance macrophage-mediated and neutrophil-mediated killing of neuroblastoma cells.[54] However, currently GM-CSF is not available in Europe, but recently G-CSF was found to be a suitable alternative (in vitro).[55] It will

be paramount to determine if one or both of these cytokines will enhance IgA3.0 ch14.18 therapy, because this is a plausible combination considering the mechanism of action. Similarly, the combination of IgA3.0 ch14.18 with 13-*cis* retinoic acid should be validated.[4] Preliminary in vitro studies already showed that combining IgA ch14.18 with GM-CSF and 13-*cis* retinoic acid enhanced ADCC of neuroblastoma cells.[13] Other combination strategies, for example, with myeloid checkpoint inhibitors like anti-CD47 antibodies could further enhance IgA3.0 ch14.18 in the future. In summary, IgA3.0 ch14.18 is a promising new therapeutic candidate to treat neuroblastoma patients, showing (1) increased half-life compared with natural IgA antibodies, (2) increased protein stability, (3) potent CD89-mediated tumor killing in vitro by healthy subjects and patients with neuroblastoma and (4) anti-tumor efficacy in long-term mouse neuroblastoma models.

Author affiliations
[1]Center for Translational Immunology, UMC Utrecht, Utrecht, The Netherlands
[2]Biomolecular Mass Spectrometry and Proteomics, Bijvoet Center for Biomolecular Research and Utrecht Institute for Biopharmaceutical Sciences, University of Utrecht, Utrecht, The Netherlands
[3]Netherlands Proteomics Center, Utrecht, The Netherlands
[4]MIlabs, Utrecht, The Netherlands
[5]Radionuclide Pharmacy, UMC Utrecht, Utrecht, The Netherlands
[6]Princess Máxima Center for Pediatric Oncology, Utrecht, The Netherlands
[7]De Boer Biotech Consultancy B.V, Blaricum, The Netherlands
[8]Section for Stem Cell Transplantation and Immunotherapy, Department of Medicine II, University Hospital Schleswig Holstein, Kiel, Germany

Twitter Albert J R Heck @hecklab

ORCID iDs
Marjolein C Stip http://orcid.org/0000-0002-5667-3402
Annelisa M Cornel http://orcid.org/0000-0001-8349-121X
Thomas Valerius http://orcid.org/0000-0001-9181-8067
Jeanette H W Leusen http://orcid.org/0000-0003-4982-6914

REFERENCES
1. De Preter K, Vandesompele J, Heimann P, *et al*. Human fetal neuroblast and neuroblastoma transcriptome analysis confirms neuroblast origin and highlights neuroblastoma candidate genes. *Genome Biol* 2006;7:R84.
2. Matthay KK, Villablanca JG, Seeger RC, *et al*. Treatment of high-risk neuroblastoma with intensive chemotherapy, radiotherapy, autologous bone marrow transplantation, and 13-cis-retinoic acid. *N Engl J Med* 1999;341:1165–73.
3. Berthold F, Boos J, Burdach S, *et al*. Myeloablative megatherapy with autologous stem-cell rescue versus oral maintenance chemotherapy as consolidation treatment in patients with high-risk neuroblastoma: a randomised controlled trial. *Lancet Oncol* 2005;6:649–58.
4. Yu AL, Gilman AL, Ozkaynak MF, *et al*. Anti-GD2 antibody with GM-CSF, interleukin-2, and isotretinoin for neuroblastoma. *N Engl J Med* 2010;363:1324–34.
5. Mueller I, Ehlert K, Endres S, *et al*. Tolerability, response and outcome of high-risk neuroblastoma patients treated with long-term infusion of anti-GD$_2$ antibody Ch14.18/CHO. *MAbs* 2018;10:55–61.
6. Bruchelt G, Handgretinger R, Kimmig A, *et al*. Effects of granulocytes on human neuroblastoma cells measured by chemiluminescence and chromium-51 release assay. *J Biolumin Chemilum* 1989;3:93–6.
7. Cheung N-K, Sowers R, Vickers AJ, *et al*. FCGR2A polymorphism is correlated with clinical outcome after immunotherapy of neuroblastoma with anti-GD2 antibody and granulocyte macrophage colony-stimulating factor. *J Clin Oncol* 2006;24:2885–90.
8. Cheung IY, Hsu K, Cheung N-K. Activation of peripheral-blood granulocytes is strongly correlated with patient outcome after immunotherapy with anti-GD2 monoclonal antibody and granulocyte-macrophage colony-stimulating factor. *J Clin Oncol* 2012;30:426–32.
9. Cheung N-K, Cheung IY, Kramer K, *et al*. Key role for myeloid cells: phase II results of anti-G(D2) antibody 3F8 plus granulocyte-macrophage colony-stimulating factor for chemoresistant osteomedullary neuroblastoma. *Int J Cancer* 2014;135:2199–205.
10. Barker E, Mueller BM, Handgretinger R, *et al*. Effect of a chimeric anti-ganglioside GD2 antibody on cell-mediated lysis of human neuroblastoma cells. *Cancer Res* 1991;51:144–9.
11. Sorkin LS, Otto M, Baldwin WM, *et al*. Anti-GD(2) with an Fc point mutation reduces complement fixation and decreases antibody-induced allodynia. *Pain* 2010;149:135–42.
12. Furman WL, Federico SM, McCarville MB, *et al*. A phase II trial of Hu14.18K322A in combination with induction chemotherapy in children with newly diagnosed high-risk neuroblastoma. *Clin Cancer Res* 2019;25:6320–8.
13. Evers M, Stip M, Keller K, *et al*. Anti-GD2 IgA kills tumors by neutrophils without antibody-associated pain in the preclinical treatment of high-risk neuroblastoma. *J Immunother Cancer* 2021;9:e003163.

14 Tsuzukida Y, Wang CC, Putnam FW. Structure of the A2m(1) allotype of human IgA--a recombinant molecule. *Proc Natl Acad Sci U S A* 1979;76:1104–8.

15 Chintalacharuvu KR, Raines M, Morrison SL. Divergence of human alpha-chain constant region gene sequences. A novel recombinant alpha 2 gene. *J Immunol* 1994;152:5299–304.

16 Mattu TS, Pleass RJ, Willis AC, *et al*. The glycosylation and structure of human serum IgA1, Fab, and Fc regions and the role of N-glycosylation on Fcα receptor interactions. *J Biol Chem* 1998;273:2260–72.

17 Blaese RM, Strober W, Levy AL, *et al*. Hypercatabolism of IgG, IgA, IgM, and albumin in the Wiskott-Aldrich syndrome. A unique disorder of serum protein metabolism. *J Clin Invest* 1971;50:2331–8.

18 Delacroix DL, Elkom KB, Geubel AP, *et al*. Changes in size, subclass, and metabolic properties of serum immunoglobulin A in liver diseases and in other diseases with high serum immunoglobulin A. *J Clin Invest* 1983;71:358–67.

19 Ovacik M, Lin K. Tutorial on monoclonal antibody pharmacokinetics and its considerations in early development. *Clin Transl Sci* 2018;11:540–52.

20 Schiff RI, Rudd C. Alterations in the half-life and clearance of IgG during therapy with intravenous gamma-globulin in 16 patients with severe primary humoral immunodeficiency. *J Clin Immunol* 1986;6:256–64.

21 Mankarious S, Lee M, Fischer S, *et al*. The half-lives of IgG subclasses and specific antibodies in patients with primary immunodeficiency who are receiving intravenously administered immunoglobulin. *J Lab Clin Med* 1988;112:634–40.

22 Boross P, Lohse S, Nederend M. Iga EGFR antibodies mediate tumour killing in vivo. *EMBO Mol Med* 2013;5:1213–26.

23 Stockert RJ, Kressner MS, Collins JC, *et al*. IgA interaction with the asialoglycoprotein receptor. *Proc Natl Acad Sci U S A* 1982;79:6229–31.

24 Rifai A, Fadden K, Morrison SL, *et al*. The N-glycans determine the differential blood clearance and hepatic uptake of human immunoglobulin (Ig)A1 and IgA2 isotypes. *J Exp Med* 2000;191:2171–82.

25 Lee SJ, Evers S, Roeder D, *et al*. Mannose receptor-mediated regulation of serum glycoprotein homeostasis. *Science* 2002;295:1898–901.

26 Goetze AM, Liu YD, Zhang Z, *et al*. High-mannose glycans on the Fc region of therapeutic IgG antibodies increase serum clearance in humans. *Glycobiology* 2011;21:949–59.

27 Brambell FW, Hemmings WA, Morris IG. A theoretical model of gamma-globulin catabolism. *Nature* 1964;203:1352–4.

28 Junghans RP, Anderson CL. The protection receptor for IgG catabolism is the beta2-microglobulin-containing neonatal intestinal transport receptor. *Proc Natl Acad Sci U S A* 1996;93:5512–6.

29 Roopenian DC, Akilesh S. FcRn: the neonatal Fc receptor comes of age. *Nat Rev Immunol* 2007;7:715–25.

30 Lohse S, Brunke C, Derer S, *et al*. Characterization of a mutated IgA2 antibody of the m(1) allotype against the epidermal growth factor receptor for the recruitment of monocytes and macrophages. *J Biol Chem* 2012;287:25139–50.

31 Brunke C, Lohse S, Derer S, *et al*. Effect of a tail piece cysteine deletion on biochemical and functional properties of an epidermal growth factor receptor-directed IgA2m(1) antibody. *MAbs* 2013;5:936–45.

32 Lohse S, Meyer S, Meulenbroek L, *et al*. An anti-EGFR IgA that displays improved pharmacokinetics and myeloid effector cell engagement in vivo. *Cancer Res* 2016;76:403–17.

33 Kiryluk K, Novak J. The genetics and immunobiology of IgA nephropathy. *J Clin Invest* 2014;124:2325–32.

34 Atkin JD, Pleass RJ, Owens RJ, *et al*. Mutagenesis of the human IgA1 heavy chain tailpiece that prevents dimer assembly. *J Immunol* 1996;157:156–9.

35 Brandsma AM, Ten Broeke T, Nederend M, *et al*. Simultaneous targeting of FcγRs and FcαRI enhances tumor cell killing. *Cancer Immunol Res* 2015;3:1316–24.

36 van Egmond M, van Vuuren AJ, Morton HC, *et al*. Human immunoglobulin A receptor (FcalphaRI, CD89) function in transgenic mice requires both FcR gamma chain and CR3 (CD11B/CD18). *Blood* 1999;93:4387–94.

37 Hamre R, Farstad IN, Brandtzaeg P, *et al*. Expression and modulation of the human immunoglobulin A Fc receptor (CD89) and the FcR gamma chain on myeloid cells in blood and tissue. *Scand J Immunol* 2003;57:506–16.

38 Huang X, Li Y, Fu M, *et al*. Polarizing macrophages in vitro. *Methods Mol Biol* 2018;1784:119–26.

39 Li F, Ulrich ML, Shih V-S, *et al*. Mouse strains influence clearance and efficacy of antibody and antibody-drug conjugate via Fc-FcγR interaction. *Mol Cancer Ther* 2019;18:780–7.

40 Mujoo K, Cheresh DA, Yang HM, *et al*. Disialoganglioside GD2 on human neuroblastoma cells: target antigen for monoclonal antibody-mediated cytolysis and suppression of tumor growth. *Cancer Res* 1987;47:1098–104.

41 Zeng Y, Fest S, Kunert R, *et al*. Anti-neuroblastoma effect of ch14.18 antibody produced in CHO cells is mediated by NK-cells in mice. *Mol Immunol* 2005;42:1311–9.

42 Siebert N, Zumpe M, von Lojewski L, *et al*. Reduction of CD11b(+) myeloid suppressive cells augments anti-neuroblastoma immune response induced by the anti-GD(2) antibody ch14.18/CHO. *Oncoimmunology* 2020;9.

43 Göritzer K, Turupcu A, Maresch D, *et al*. Distinct Fcα receptor *N*-glycans modulate the binding affinity to immunoglobulin A (IgA) antibodies. *J Biol Chem* 2019;294:13995–4008.

44 Göritzer K, Maresch D, Altmann F, *et al*. Exploring site-specific N-glycosylation of HEk293 and plant-produced human IgA isotypes. *J Proteome Res* 2017;16:2560–70.

45 Zhong X, Ma W, Meade CL, *et al*. Transient CHO expression platform for robust antibody production and its enhanced N-glycan sialylation on therapeutic glycoproteins. *Biotechnol Prog* 2019;35:e2724.

46 Rouwendal GJ, van der Lee MM, Meyer S, *et al*. A comparison of anti-HER2 IgA and IgG1 in vivo efficacy is facilitated by high N-glycan sialylation of the IgA. *MAbs* 2016;8:74–86.

47 Steffen U, Koeleman CA, Sokolova MV, *et al*. Iga Subclasses have different Effector functions associated with distinct Glycosylation profiles. *Nat Commun* 2020;11:120.

48 Snoeck V, Peters IR, Cox E. The IgA system: a comparison of structure and function in different species. *Vet Res* 2006;37:455–67.

49 Andersen JT, Daba MB, Berntzen G, *et al*. Cross-species binding analyses of mouse and human neonatal Fc receptor show dramatic differences in immunoglobulin G and albumin binding. *J Biol Chem* 2010;285:4826–36.

50 Sharma SK, Chow A, Monette S, *et al*. Fc-mediated anomalous biodistribution of therapeutic antibodies in immunodeficient mouse models. *Cancer Res* 2018;78:1820–32.

51 Kendra K, Malkovska V, Allen M, *et al*. In vivo binding and antitumor activity of ch14.18. *J Immunother* 1999;22:423–30.

52 Barry WE, Jackson JR, Asuelime GE, *et al*. Activated natural killer cells in combination with anti-GD2 antibody dinutuximab improve survival of mice after surgical resection of primary neuroblastoma. *Clin Cancer Res* 2019;25:325–33.

53 Zhang D, Chen G, Manwani D, *et al*. Neutrophil ageing is regulated by the microbiome. *Nature* 2015;525:528–32.

54 Batova A, Kamps A, Gillies SD, *et al*. The ch14.18-GM-CSF fusion protein is effective at mediating antibody-dependent cellular cytotoxicity and complement-dependent cytotoxicity in vitro. *Clin Cancer Res* 1999;5:4259–63.

55 Martinez Sanz P, van Rees DJ, van Zogchel LMJ, *et al*. G-CSF as a suitable alternative to GM-CSF to boost dinutuximab-mediated neutrophil cytotoxicity in neuroblastoma treatment. *J Immunother Cancer* 2021;9:e002259.

Supplemental Methods

Mass spectrometry for glycosylation analysis

Unless otherwise stated, chemicals and reagents were acquired from Sigma Aldrich. 10 µg of antibody was denatured, reduced and alkylated by adding 100 µL of 150 mM Tris, 5mM TCEP, 30 mM CAA, 1% SDC, at pH 8,5. Next, 100 ng GluC (Roche) was added and the sample was incubated at 37 °C for 4 h. Hereafter, 100 ng of trypsin was added and the sample was incubated overnight at 37 °C. The samples where then acidified by adding TFA to a concentration of 0.5%, causing SDC to precipitate, followed by solid phase extraction (SPE) using an Oasis HBL µ-elution plate (Waters Chromatography). After SPE, the samples where dried with a vacuum centrifuge. Subsequently the sample was reconstituted in 2% FA.

Samples were analyzed on a Fusion Lumos mass spectrometer (ThermoFischer) connected to a UHPLC 3000 system (ThermoFischer). Approximately 100 ng of reconstituted peptides were trapped on a precolumn and then separated on a 50 cm x 75 µm Poroshell EC-C18 analytical column (2.7 µm) temperature controlled at 40 °C. Solvent A consisted of 0.1% formic acid, solvent B of 0.1% formic acid in 80% acetonitrile. Trapping was performed for 2 min in 9% solvent B. Peptides were separated by a 40 min gradient of 9–44% buffer B followed by 44–99% B in 4 min, 99% B for 10 min. MS data were obtained in data-dependent acquisition mode with three separate fragmentation modes: higher-energy collisional dissociation (HCD), HCD-product-dependent stepping collision energy HCD (HCD-pd-sHCD) and HCD-product-dependent electron-transfer/higher-energy collision dissociation (HCD-pd-EtHCD). For all three methods, full scans were acquired in the *m/z* range of 350-2000 at a resolution of 120,000 (at *m/z* 400) with AGC target $3*10^6$. In the runs the most intense precursor ions were selected for HCD fragmentation performed at a normalized collision energy (NCE) of 29%, after accumulation to target value of $1*10^5$. MS/MS acquisition was performed at a resolution of 60,000, recording within an *m/z* window from 120-4000. Product-dependent fragmentation methods were initiated when at least three of the following ions (± 20 ppm) were detected from the preceding HCD scan: 127.0390, 138.0550, 145.0495, 163.0601, 168.0655, 186.0761, 204.0867, 243.0264, 274.0921, 292.1027, 366.1395, 405.0793, 407.1660, 512.1974, or 657.2349. HCD-pd-sHCD was performed with NCEs at 10%, 25% and 40%, whereas HCD-pd-EThcD made use of supplemental activation at 25%.

The MS data were searched using Byonic v4.1.10 (Protein Metrics Inc), with a fully specific search for C-terminal cleavage at Arg, Lys, Glu and Asp, with a maximum of three missed cleavages. Precursor mass tolerance was set at 10 ppm and fragment mass tolerance (both HCD and EThcD) at 20 ppm. Cys carbamidomethylation was set as fixed modification, with variable modifications including oxidation, pyroglutamic acid formation and phosphorylation, in addition to 279 potential *N*-glycan species. Detections were filtered for having a Byonic score ≥150 and a |log| peptide probability score ≥1.5. Subsequently, we used Skyline (21.1.0.146) to integrate the MS1 areas of the resulting list of glycan composition for the most frequently occurring peptide sequences. For this, we allowed a 5 ppm mass accuracy for the glycopeptide combination and filtered on having a dotp of 0.8 for the best replicate. Integration windows were manually adjusted to capture the whole peak area for a signal, and to have overlapping retention times in the MS1 replicates. Integrated areas were normalized to the sum of intensities per peptide. For visualization of glycans recommendations of the Consortium for Functional Glycomics were followed and glycan cartoons were constructed using GlycoWorkbench (v2.1 build 146).

Indium-111 labeling and biodistribution SPECT/CT scans

IgG1 and IgA3.0 ch14.18 (500ug, 1mg/mL) were transferred to 0.1 M sodium bicarbonate (pH 8.2) buffer using 30kDa Amicon Ultra 0.5 mL centrifugal filters (Merck). A 20-fold molar excess of p-SCN-Bn-DTPA metal linker (2 mg/mL in dry DMSO, Macrocyclics) was added and incubated for 1 h at 37 °C. Samples were passed through a G50 Sephadex column, eluted with 0.5 M MES (2-(*N*-morpholino)ethanesulfonic acid) buffer (pH 5.4, Sigma) and fractions containing BnDTPA-antibody conjugates were collected. BnDTPA-antibodies were transferred to 0.5 M MES buffer using 30 kDa centrifugal filters as above. 150 µL Indium-111 (activity of 370 MBq/mL, Mallinckrodt) was added per 150 µg BnDTPA-antibody sample and incubated for 1 h at RT. Samples were passed through a G50 column, eluted with PBS (pH 7.4) and fractions containing ^{111}In-labeled antibody were collected. Purity was assessed by running samples with 0.1 M citrate buffer on an iTLC (instant Thin-Layer Chromatography) strip (Agilent) followed by radio-TLC scanning. Purity for both IgA3.0 and IgG1 was over 97% (**Suppl. Fig. 5D**).

NSG mice with s.c. IMR32 tumors (+/- 1500 mm3) were injected i.v. with either 1.6 MBq ^{111}In-labeled IgG1 or 3.2 MBq ^{111}In-labeled IgA3.0 ch14.18. SPECT/CT images were acquired in list-mode at 24 h and 48 h post-injection using a VECTor6CT (MILabs B.V., Utrecht, NL). All animals were anaesthetized using 4% isoflurane and maintained at 2% and 37 °C throughout the imaging session. Image acquisition was performed using the HE-UHR-M collimator (0.75 mm pinhole size) for approximately 1 h. Total-body CT images were acquired for anatomical reference and attenuation correction (50 kvP, 0.21 mA, 75 ms). Reconstruction of SPECT images was performed using the SROSEM algorithm (5 iterations, 128 subsets, and 0.2 mm voxel size) and an automatic triple energy window for scatter correction at both photopeaks of ^{111}In. Reconstruction of CT images was performed at 100 μm as per manufacturers' default settings. To allow quantification of SPECT data, calibration factors derived from ^{111}In phantoms were used and for attenuation correction the SPECT data was registered to the CT data. Image post-processing was performed using the volume-of-interest analyses with the PMOD software package (Version 4.1, PMOD Technologies) to calculate the % injected dose per mL of tissue (% ID/mL).

Supplemental Tables

Marker	Fluorochrome	Clone	Dilution	Company
CD45	BV510	HI30	1:200	Biolegend
CD14	FITC	TÜK4	1:50	Miltenyi
CD3	PB	UCHT1	1:50	BD
CD20	APC-H7	2H7	1:100	BD
CD56	PE-Cy7	NCAM 16.2	1:200	BD
CD16	PE	3G8	1:100	BD

Supplemental table 1 | Panel of fluorophore-conjugated antibodies for human PBMC analysis

Marker	Fluorochrome	Clone	Dilution	Company
CD45	BV510	HI30	1:200	Biolegend
CD66b	AF647	G10F5	1:400	Biolegend
CD89	PerCP-Cy5.5	A59	1:80	Biolegend
LOX-1	PE	15C4	1:50	Biolegend
CD11b	APC-Cy7	ICRF44	1:100	Biolegend

Supplemental table 2 | Panel of fluorophore-conjugated antibodies for human PMN analysis

Marker	Fluorochrome	Clone	Dilution	Company
c-kit	BV711	2B8	1:50	BD
CD45	BV510	30-F11	1:200	Biolegend
CD11b	FITC	M1/70	1:50	BD
F4/80	BV781	BM8	1:200	Biolegend
Human CD89	PE	A59	1:50	BD
Ly6C	PerCP-Cy5.5	HK1.4	1:100	Biolegend
Ly6G	PE-Cy7	1A8	1:200	Biolegend
Siglec F (CD170)	BV421	S17007L	1:50	Biolegend

Supplemental table 3 | Panel of fluorophore-conjugated antibodies for mouse tissue analysis with flow cytometry

Supplemental material

BMJ Publishing Group Limited (BMJ) disclaims all liability and responsibility arising from any reliance placed on this supplemental material which has been supplied by the author(s)

J Immunother Cancer
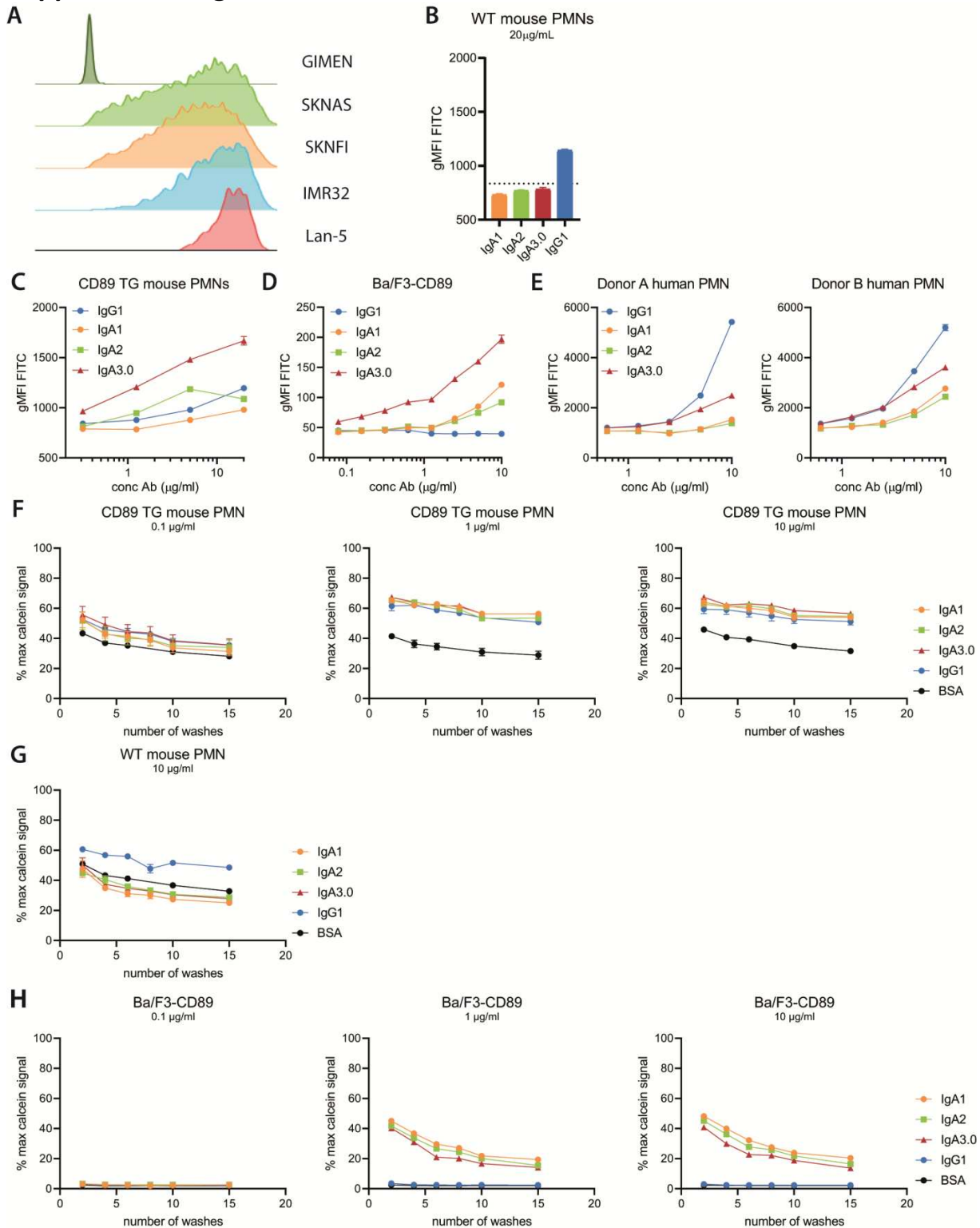
Supplemental Figures

Figure S1 | GD2 expression and ch14.18 antibody binding (**A**) GD2 expression on neuroblastoma cell lines determined with flow cytometry. Monomeric Fc-binding to CD89 was assessed by incubating ch14.18 antibodies with (**B**) WT mouse PMN, (**C**) CD89 transgenic mouse neutrophils, (**D**) Ba/F3-CD89 cells or (**E**) human PMN followed by detection with FITC anti-human kappa antibody. Binding of complexed IgA to CD89 was assessed by incubating calcein-labeled (**F**) CD89 transgenic mouse PMN, (**G**) wild type mouse PMN or (**H**) Ba/F3-CD89 cells with antibody-coated plates and measuring remaining fluorescence during 10 washes. PMN = polymorphonuclear leukocytes.
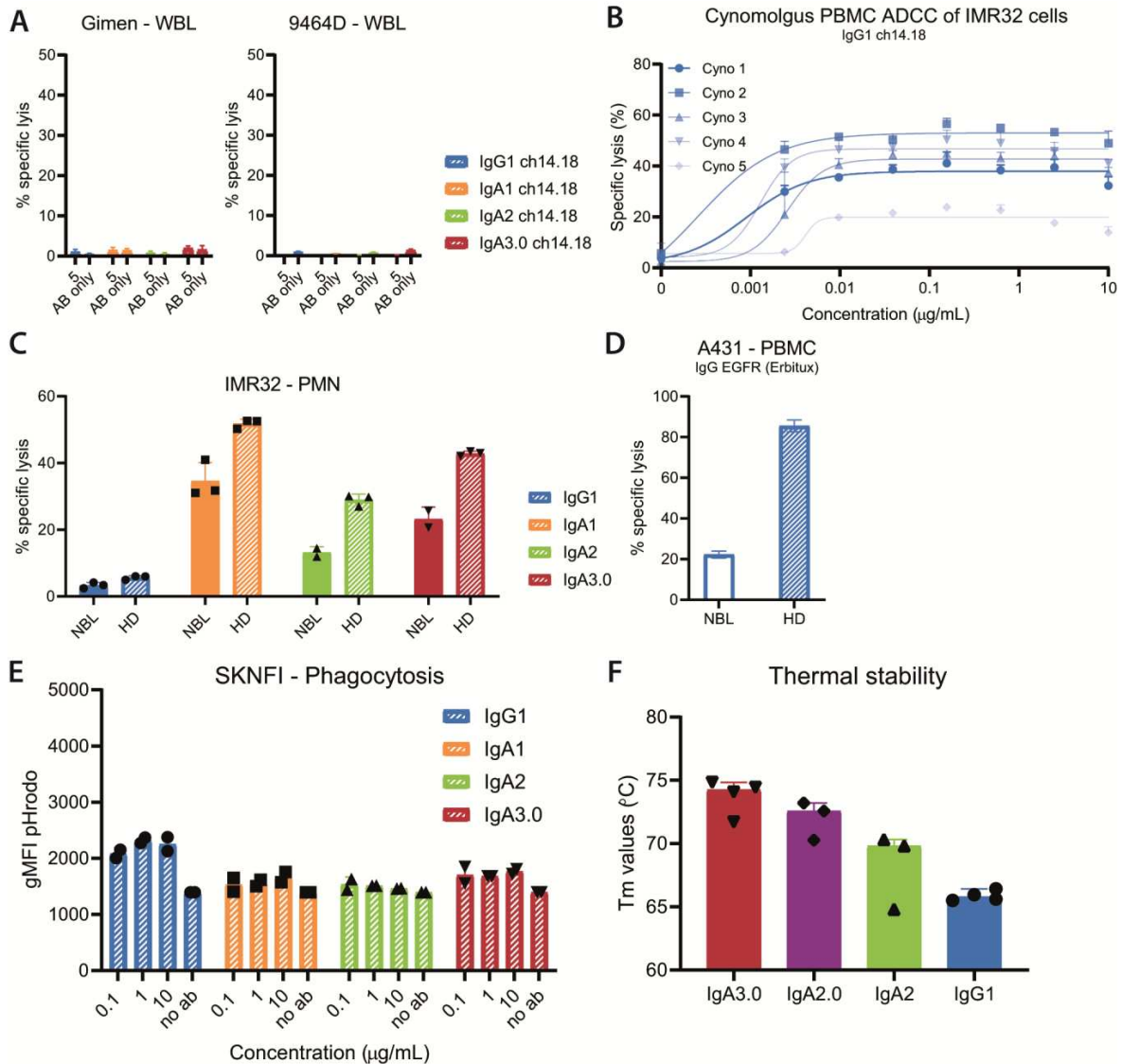
4

Figure S2 | ADCC and ADCP experiments and Tm values in thermal stability assays. (**A**) ADCC against GD2-negative neuroblastoma target cells was studied in ^{51}Cr-release assays with WBL as effector cells. (**B**) ^{51}Cr-release assays with cynomolgus PBMC as effector cells. (**C**) Comparison of neuroblastoma patient-derived PMN and healthy donor PMN ADCC against IMR32 cells upon IgA3.0 ch14.18 stimulation in ^{51}Cr-release assays. (**D**) Comparison of neuroblastoma patient-derived PBMC and healthy donor PBMC ADCC against A431 cells upon IgG EGFR (Erbitux) stimulation in ^{51}Cr-release assays. (**E**) The efficiency of antibodies in inducing ADCP against pHrodo-labeled human neuroblastoma target cells was assessed with monocyte-derived macrophages differentiated with M-CSF as effector cells. (**F**) Average Tm values as determined by Sypro orange thermal shift assays for different isotypes of 2D11 (anti-CD47), Obinutuzumab (anti-CD20), Rituximab (anti-CD20), Dinutuximab (anti-GD2), Trastuzumab (anti-Her2) and Cetuximab (anti-EGFR) antibodies. PMN = polymorphonuclear leukocytes, PBMC = peripheral blood mononuclear cells, WBL = whole blood leukocytes.
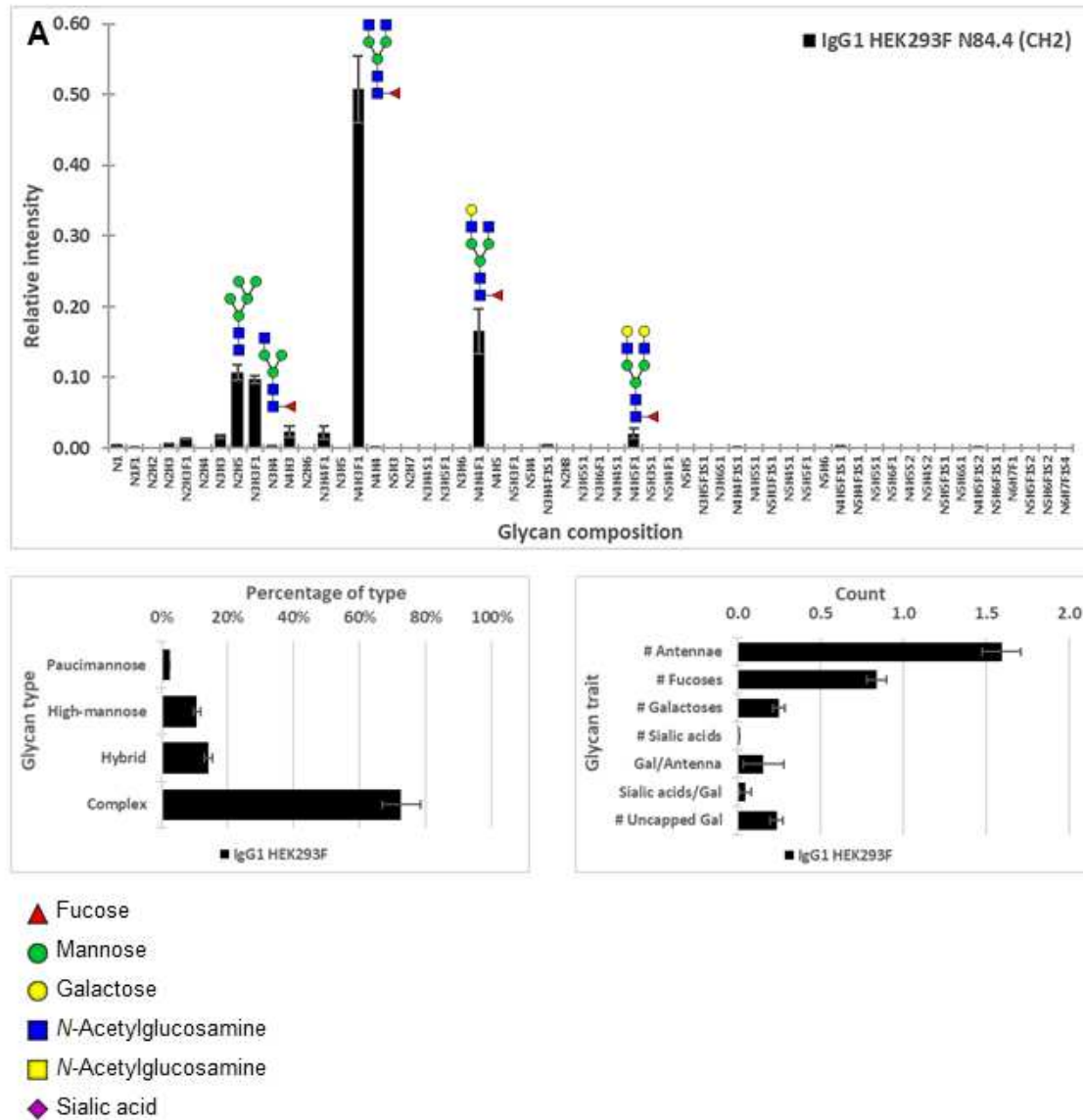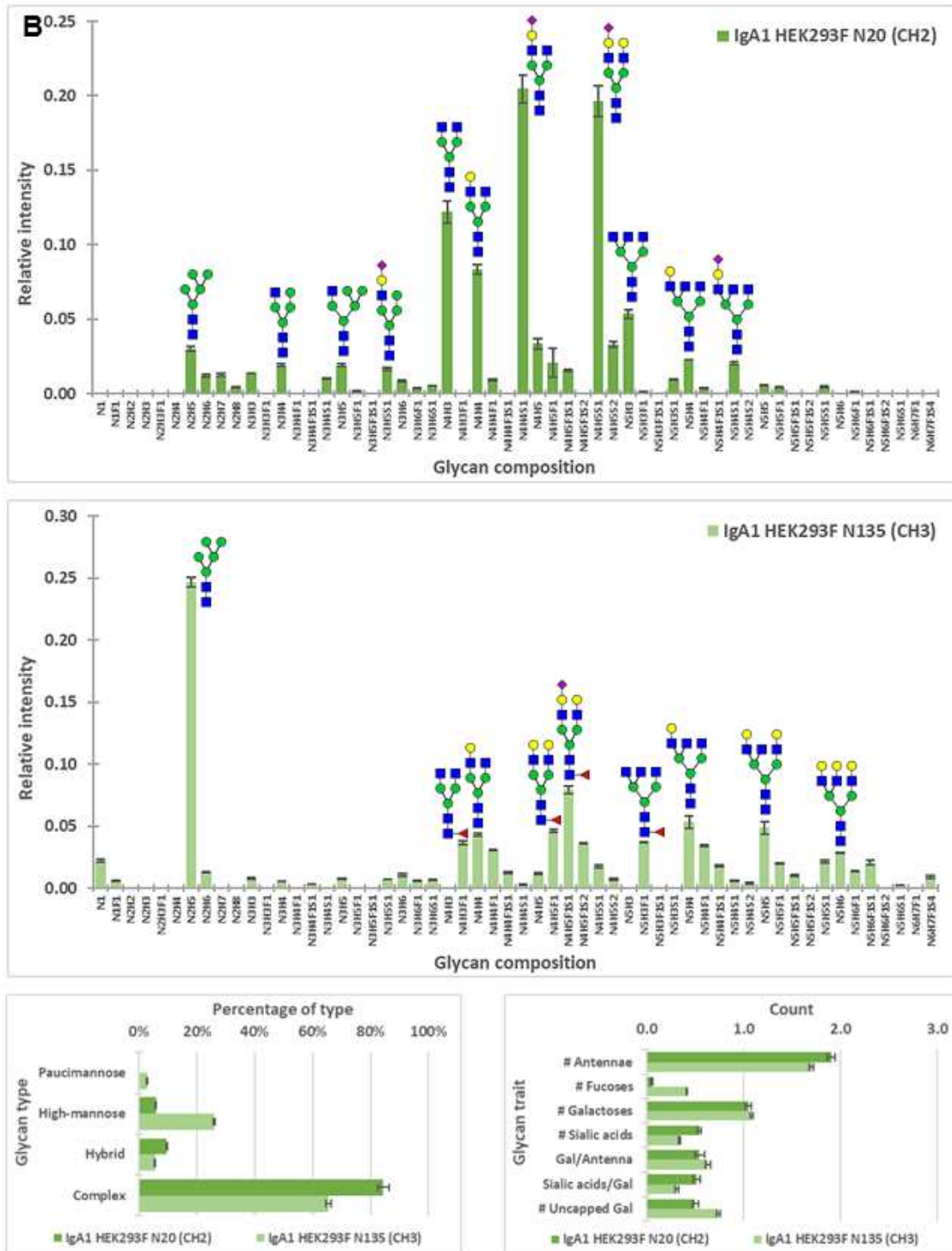
5

Figure S3 | Glycosylation analysis. Complete glycosylation profiles of IgG1 (**A**), IgA1 (**B**), IgA2 (**C**) and IgA3.0 (**D**) ch14.18 antibodies.
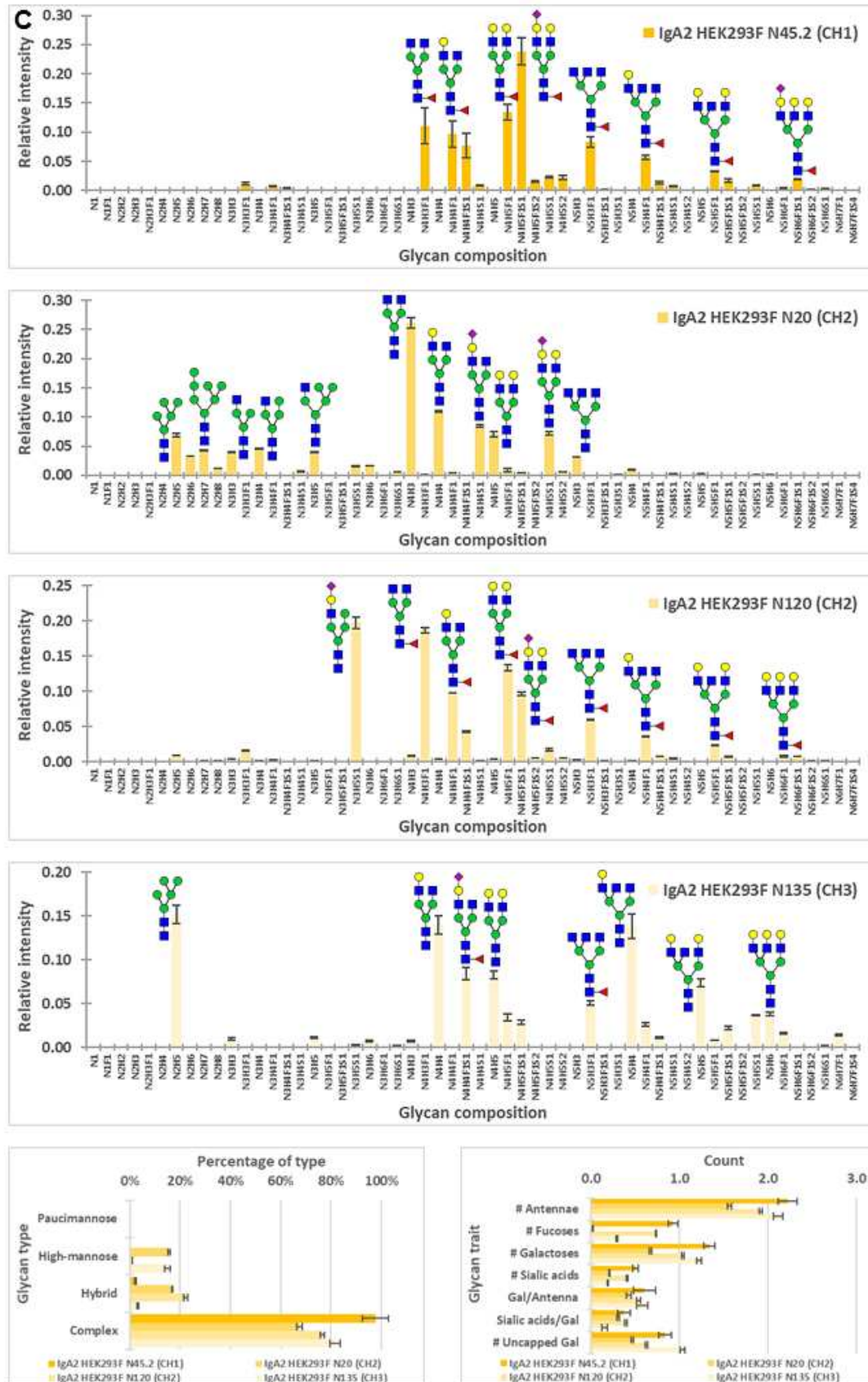
6

Figure S3 | Glycosylation analysis. Complete glycosylation profiles of IgG1 (**A**), IgA1 (**B**), IgA2 (**C**) and IgA3.0 (**D**) ch14.18 antibodies.

7

Supplemental material

BMJ Publishing Group Limited (BMJ) disclaims all liability and responsibility arising from any reliance placed on this supplemental material which has been supplied by the author(s)

J Immunother Cancer

Figure S3 | Glycosylation analysis. Complete glycosylation profiles of IgG1 (**A**), IgA1 (**B**), IgA2 (**C**) and IgA3.0 (**D**) ch14.18 antibodies.
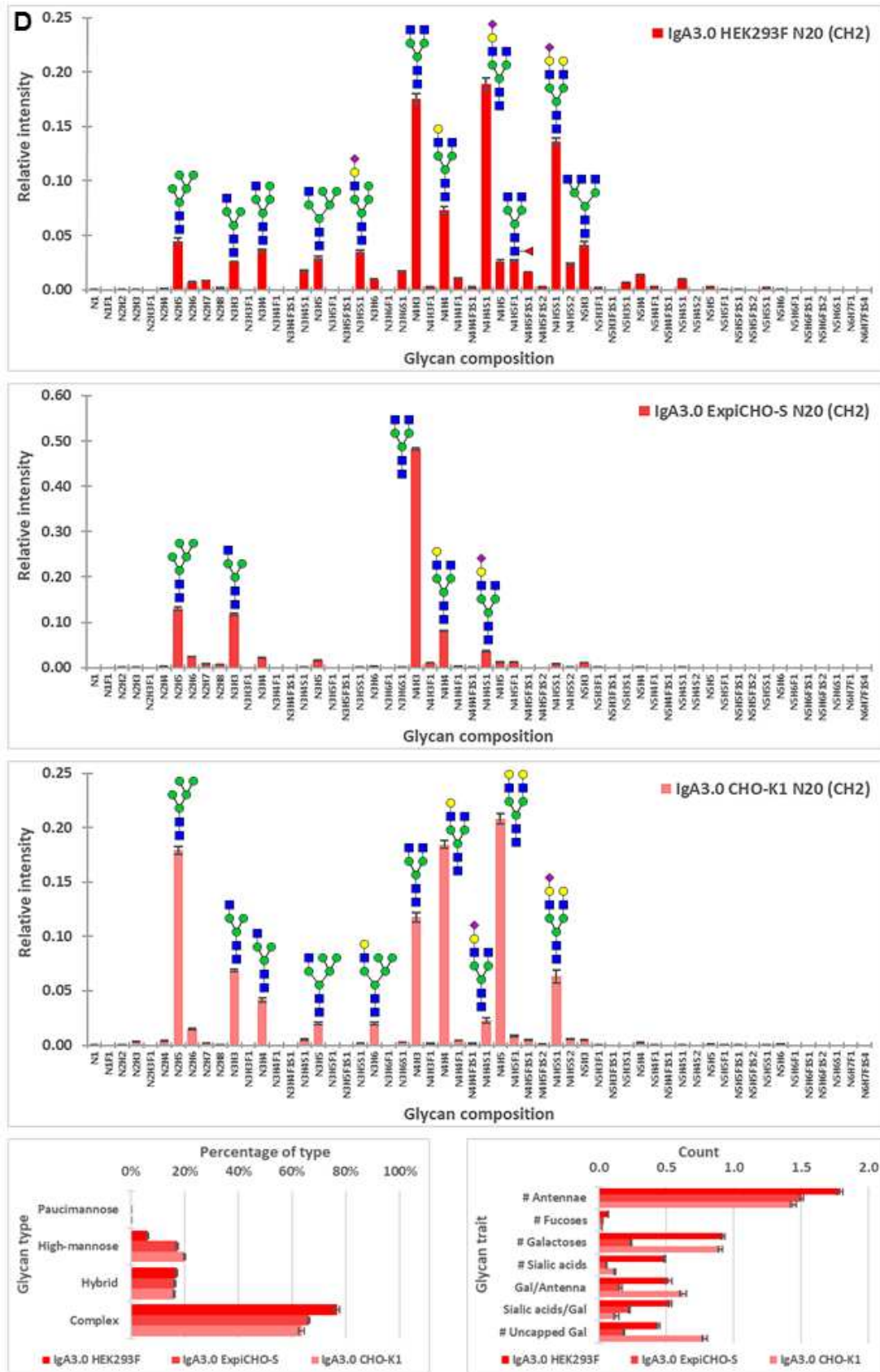
8

Figure S3 | Glycosylation analysis. Complete glycosylation profiles of IgG1 (**A**), IgA1 (**B**), IgA2 (**C**) and IgA3.0 (**D**) ch14.18 antibodies.
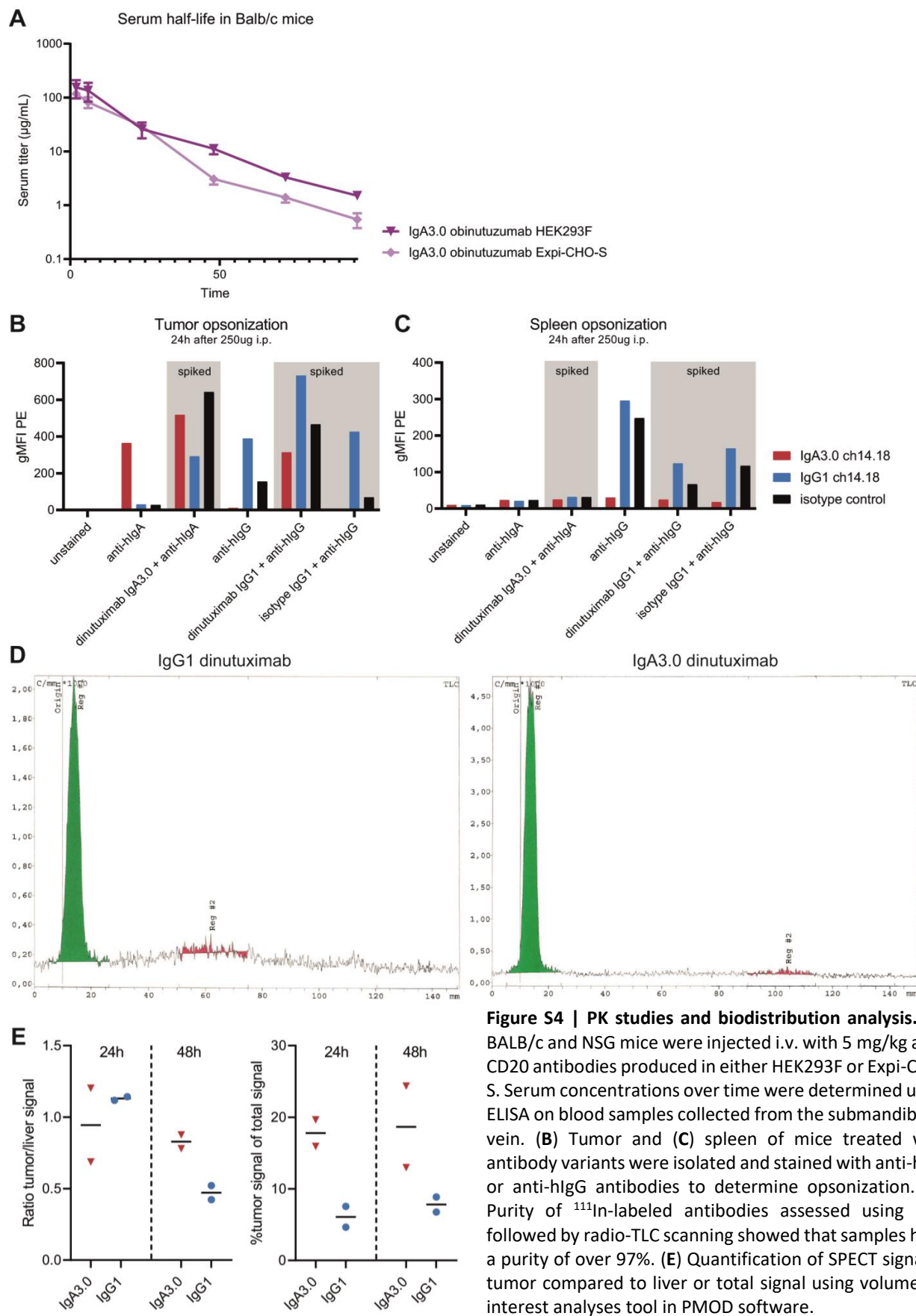
9

Figure S4 | PK studies and biodistribution analysis. (A) BALB/c and NSG mice were injected i.v. with 5 mg/kg anti-CD20 antibodies produced in either HEK293F or Expi-CHO-S. Serum concentrations over time were determined using ELISA on blood samples collected from the submandibular vein. **(B)** Tumor and **(C)** spleen of mice treated with antibody variants were isolated and stained with anti-hIgA or anti-hIgG antibodies to determine opsonization. **(D)** Purity of ^{111}In-labeled antibodies assessed using iTLC followed by radio-TLC scanning showed that samples have a purity of over 97%. **(E)** Quantification of SPECT signal in tumor compared to liver or total signal using volume-of-interest analyses tool in PMOD software.
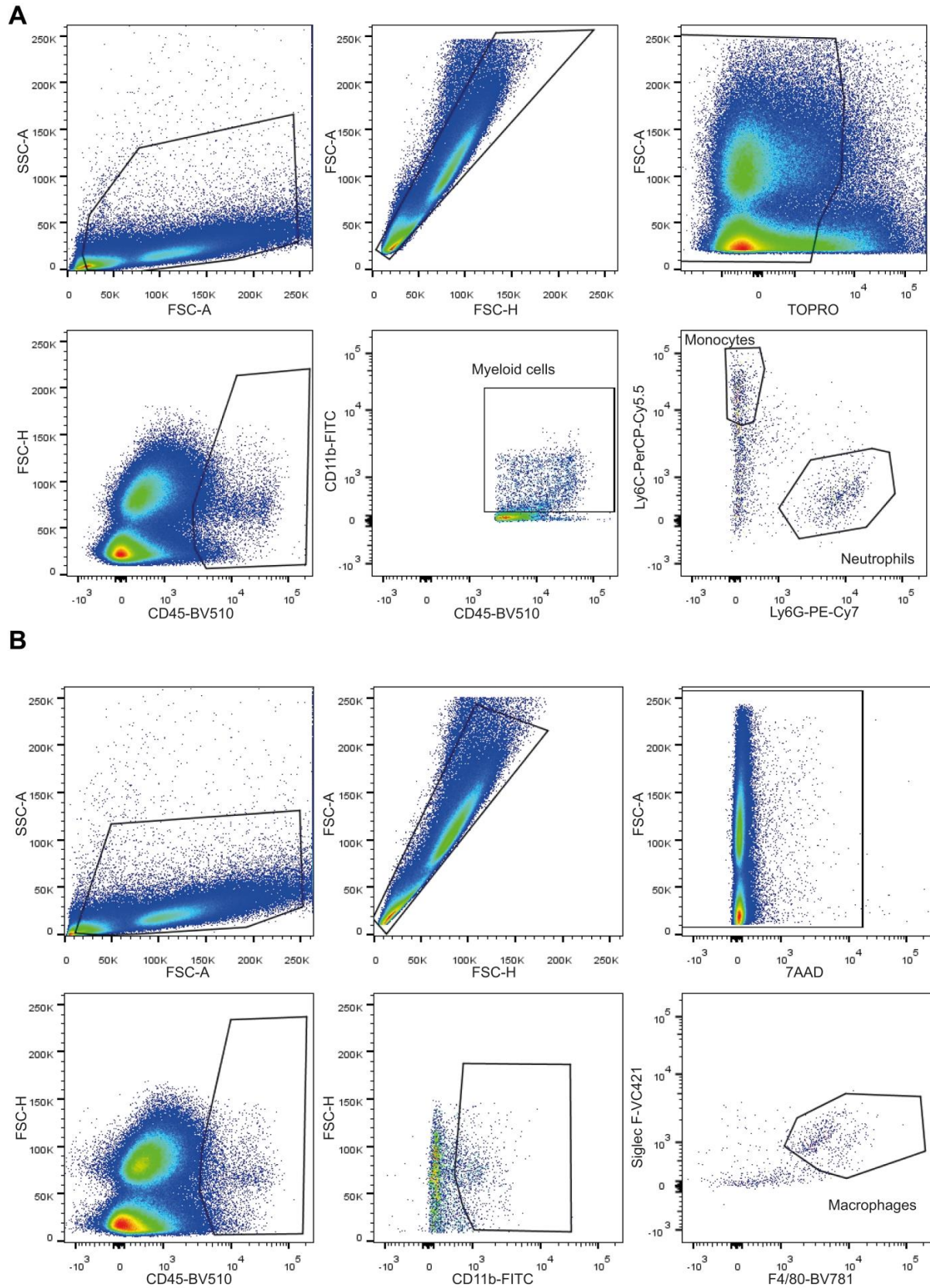
10

Figure S5 | Gating strategies for immune cell populations in IMR32 tumors. (A) Gating strategy for CD11b⁺ myeloid cells, Ly6G⁺ Ly6C^int neutrophils and Ly6C^high monocytes in IMR32 tumors. **(B)** Gating strategy for F4/80⁺ macrophages in IMR32 tumors.

11

Supplemental material

BMJ Publishing Group Limited (BMJ) disclaims all liability and responsibility arising from any reliance placed on this supplemental material which has been supplied by the author(s)
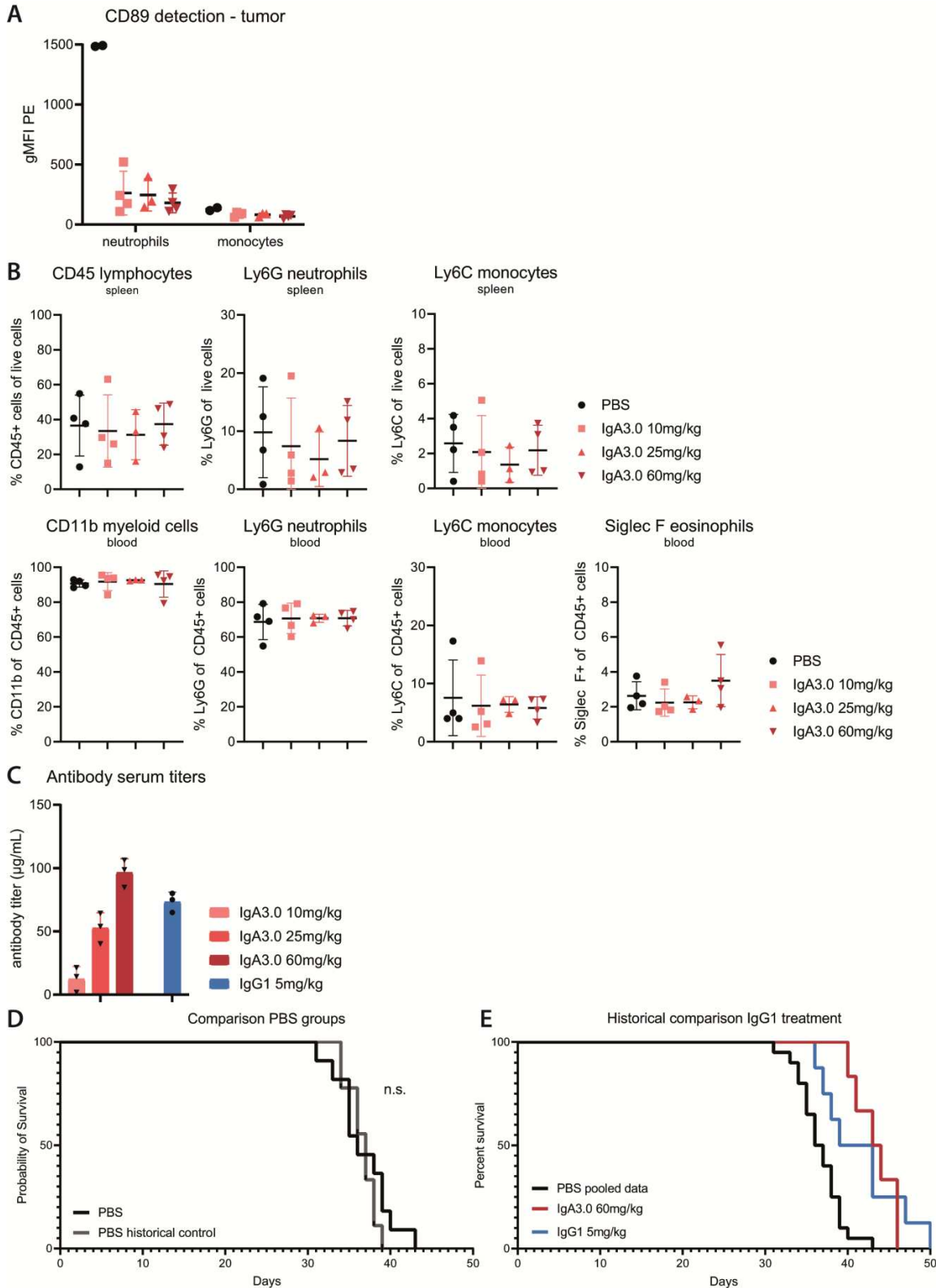
J Immunother Cancer

Figure S6 | TME analysis, serum antibody titers in IMR32 tumor bearing mice and historical comparison of IgA3.0 ch14.18 with IgG1 ch14.18 therapy. (**A**) CD89 staining on neutrophils and monocytes in tumor samples. (**B**) Spleen and blood immune cell composition of IMR32 tumor bearing mice. (**C**) Serum concentrations were determined using ELISA on blood samples collected from the submandibular vein. (**D**) Historical comparison of PBS groups from 2 different experiments shows similar outgrowth of IMR32 tumors in NSG mice. (**E**) Historical comparison of treatment with 60 mg/kg IgA3.0 ch14.18 or 5 mg/kg IgG1 ch14.18 showed similar therapeutic effects of antibodies.
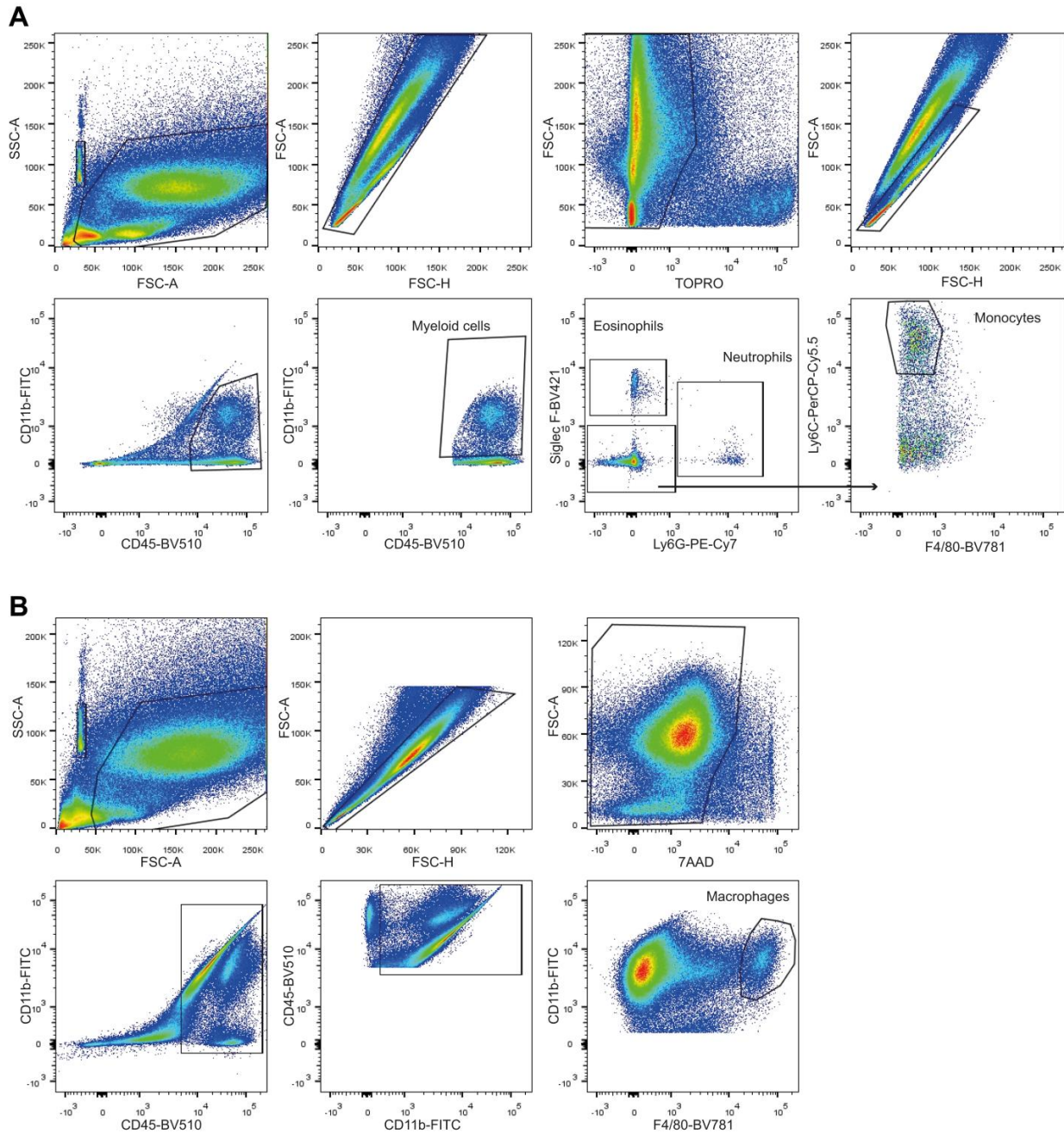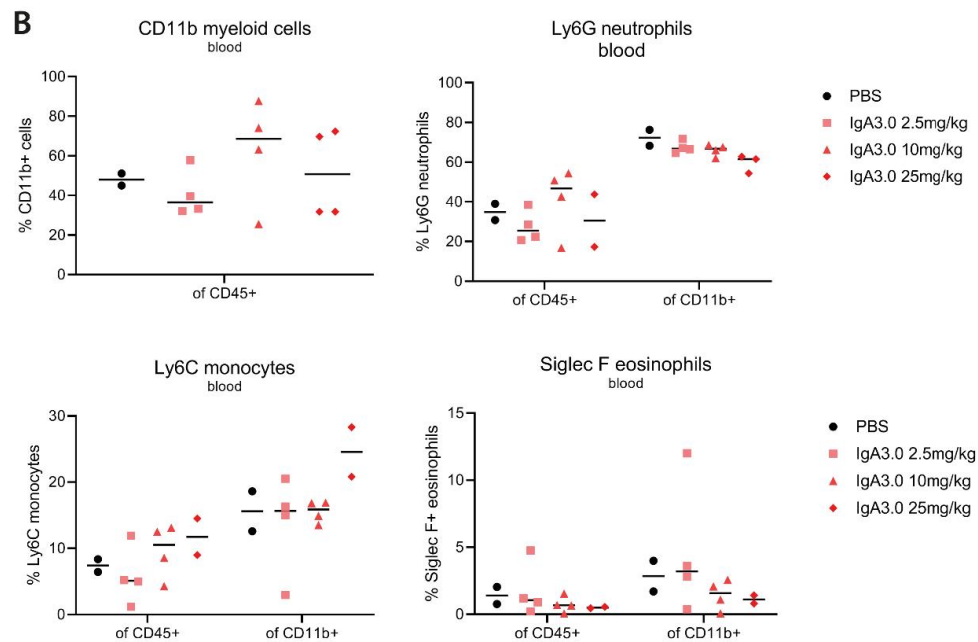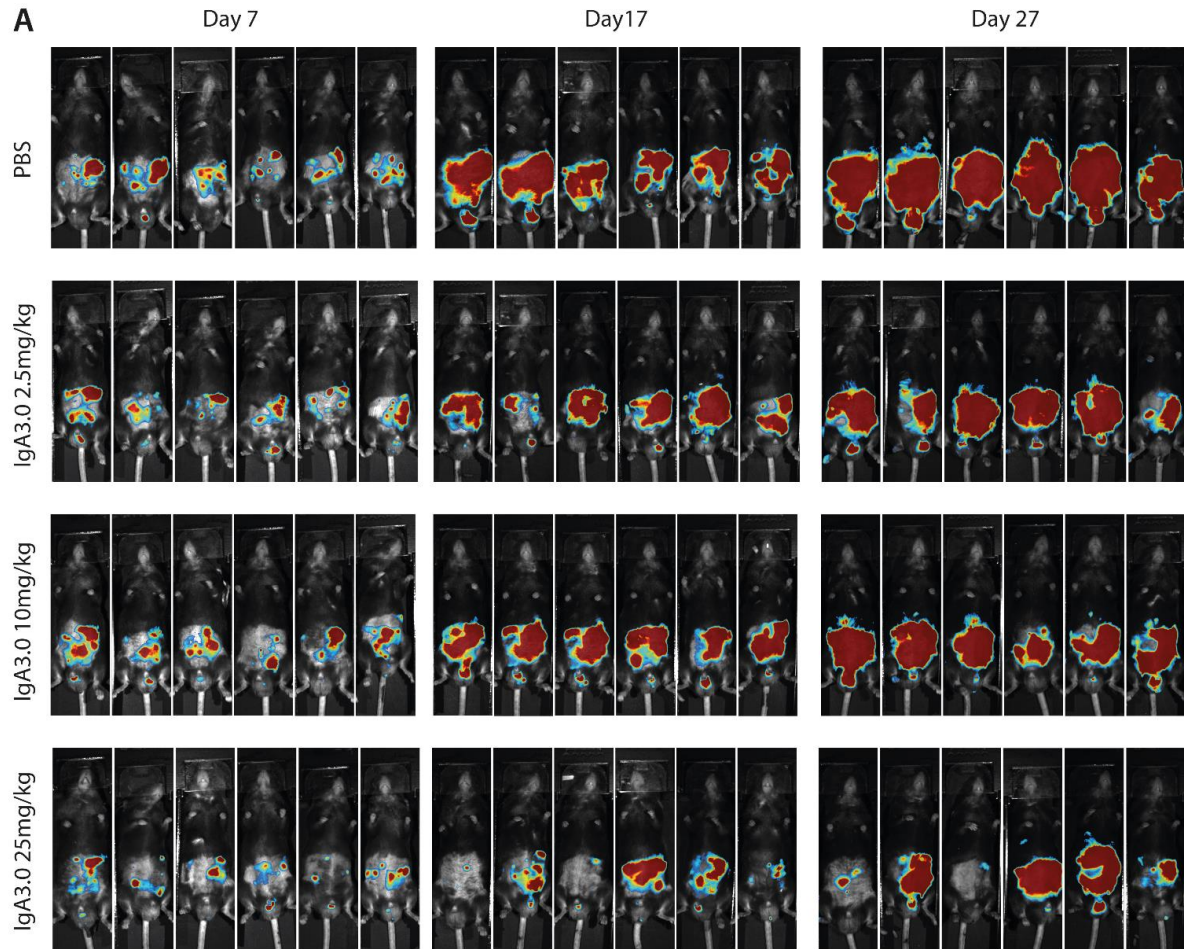
Supplemental material

BMJ Publishing Group Limited (BMJ) disclaims all liability and responsibility arising from any reliance placed on this supplemental material which has been supplied by the author(s)

J Immunother Cancer

Figure S7 | Gating strategies for immune cell populations in 9464D-GD2 tumors. (**A**) Gating strategy for CD11b$^+$ myeloid cells, Ly6G$^+$ Ly6C^{int} neutrophils, Siglec F$^+$ eosinophils and Ly6C^{high} monocytes in 9464D-GD2 tumors. (**B**) Gating strategy for F4/80$^+$ macrophages in 9464D-GD2 tumors.

13

Supplemental material

BMJ Publishing Group Limited (BMJ) disclaims all liability and responsibility arising from any reliance placed on this supplemental material which has been supplied by the author(s)
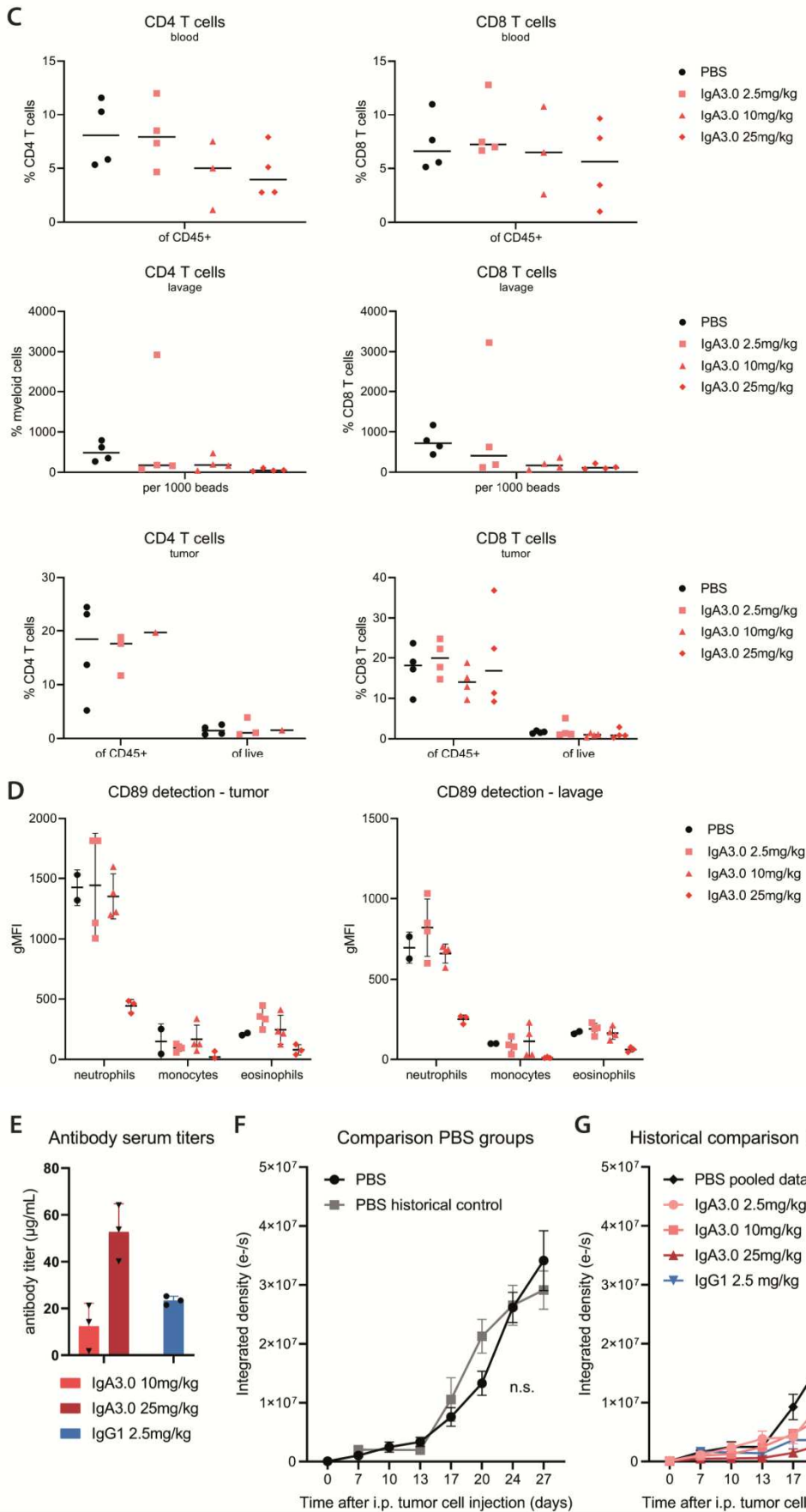
J Immunother Cancer

Figure S8 | BLI scans of 9464D-GD2 tumor outgrowth, TME analysis, serum antibody titers and historical comparison of IgA3.0 ch14.18 with IgG1 ch14.18 therapy. (**A**) BLI scans with photo overlay of 9464D-GD2 tumor outgrowth in C57Bl/6 mice. (**B**) Blood immune cell composition of 9464D-GD2 tumor bearing mice. (**C**) T cell quantification in blood, peritoneal lavage and tumor samples of 9464D-GD2 tumor bearing mice. (**D**) CD89 staining on neutrophils, monocytes and eosinophils in tumor and peritoneal lavage samples. (**E**) Serum concentrations were determined using ELISA on blood samples collected from the submandibular vein (**F**) Historical comparison of PBS groups from 2 different experiments shows similar outgrowth of 9464D-GD2 tumors in C57BL/6 mice. (**G**) Historical comparison of treatment with IgA3.0 and IgG1 ch14.18 showed similar therapeutic efficacy.